Cell

Article

A basophil-neuronal axis promotes itch

Graphical Abstract

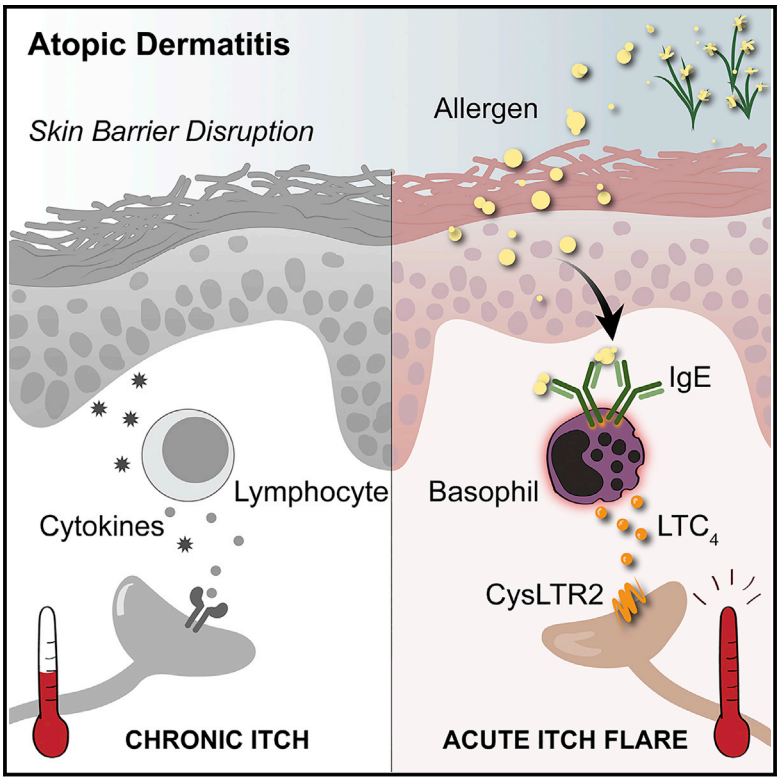

Highlights

- Heterogeneous forms of itch underlie atopic dermatitis
- Basophils promote a mast cell-independent form of IgE-mediated itch
- Allergen-stimulated basophils release leukotriene C4 and interact with sensory nerves
- Leukotriene C4-CysLTR2 neuronal signaling mediates acute itch flares

Authors

Fang Wang, Anna M. Trier, Fengxian Li, ..., Marius Ardeleanu, Mark J. Miller, Brian S. Kim

Correspondence

briankim@wustl.edu

In Brief

Wang et al. show atopic dermatitis-associated inflammation promotes a basophil-leukotriene neuroimmune axis to evoke acute itch flares.

Wang et al., 2021, Cell *184*, 1–19
January 21, 2021 © 2020 Elsevier Inc.
https://doi.org/10.1016/j.cell.2020.12.033

CellPress

Please cite this article in press as: Wang et al., A basophil-neuronal axis promotes itch, Cell (2021), https://doi.org/10.1016/j.cell.2020.12.033

Cell

CellPress

Article

A basophil-neuronal axis promotes itch

Fang Wang,[1,2,3] Anna M. Trier,[1,2] Fengxian Li,[2,4,16] Seonyoung Kim,[5] Zhen Chen,[6] Jiani N. Chai,[7] Madison R. Mack,[1,2,17] Stephanie A. Morrison,[1,2] Jennifer D. Hamilton,[6] Jinok Baek,[1,8] Ting-Lin B. Yang,[1,2] Aaron M. Ver Heul,[2,9] Amy Z. Xu,[1,2] Zili Xie,[2,16] Xintong Dong,[10,11] Masato Kubo,[12,13] Hongzhen Hu,[2,16] Chyi-Song Hsieh,[7,14] Xinzhong Dong,[10,11] Qin Liu,[2,16] David J. Margolis,[15] Marius Ardeleanu,[6] Mark J. Miller,[5] and Brian S. Kim[1,2,7,16,18,*]

[1]Division of Dermatology, Department of Medicine, Washington University School of Medicine, St. Louis, MO 63110, USA
[2]Center for the Study of Itch and Sensory Disorders, Washington University School of Medicine, St. Louis, MO 63110, USA
[3]Department of Dermatology, The First Affiliated Hospital, Sun Yat-sen University, Guangzhou, Guangdong 510080, China
[4]Department of Anesthesiology, Zhujiang Hospital of Southern Medical University, Guangzhou, Guangdong 510282, China
[5]Division of Infectious Diseases, Department of Internal Medicine, Washington University School of Medicine, St. Louis, MO 63110, USA
[6]Regeneron Pharmaceuticals, Inc., Tarrytown, NY 10591, USA
[7]Department of Pathology and Immunology, Washington University School of Medicine, St. Louis, MO 63110, USA
[8]Department of Dermatology, College of Medicine, Gachon University, Incheon 21565, Korea
[9]Division of Allergy and Immunology, Department of Medicine, Washington University School of Medicine, St. Louis, MO 63110, USA
[10]The Solomon H. Snyder Department of Neuroscience, Johns Hopkins University School of Medicine, Baltimore, MD 21205, USA
[11]Howard Hughes Medical Institute, Johns Hopkins University School of Medicine, Baltimore, MD 21205, USA
[12]Laboratory for Cytokine Regulation, Center for Integrative Medical Science, RIKEN Yokohama Institute, Yokohama 230-0045, Kanagawa Prefecture, Japan
[13]Division of Molecular Pathology, Research Institute for Biomedical Science, Tokyo University of Science, Noda 278-0022, Chiba Prefecture, Japan
[14]Division of Rheumatology, Department of Internal Medicine, Washington University School of Medicine, St. Louis, MO 63110, USA
[15]Department of Dermatology, University of Pennsylvania Perelman School of Medicine, Philadelphia, PA 19104, USA
[16]Department of Anesthesiology, Washington University School of Medicine, St. Louis, MO 63110, USA
[17]Present address: Immunology and Inflammation Therapeutic Area, Sanofi, Cambridge, MA 02139, USA
[18]Lead contact
*Correspondence: briankim@wustl.edu
https://doi.org/10.1016/j.cell.2020.12.033

SUMMARY

Itch is an evolutionarily conserved sensation that facilitates expulsion of pathogens and noxious stimuli from the skin. However, in organ failure, cancer, and chronic inflammatory disorders such as atopic dermatitis (AD), itch becomes chronic, intractable, and debilitating. In addition to chronic itch, patients often experience intense acute itch exacerbations. Recent discoveries have unearthed the neuroimmune circuitry of itch, leading to the development of anti-itch treatments. However, mechanisms underlying acute itch exacerbations remain overlooked. Herein, we identify that a large proportion of patients with AD harbor allergen-specific immunoglobulin E (IgE) and exhibit a propensity for acute itch flares. In mice, while allergen-provoked acute itch is mediated by the mast cell-histamine axis in steady state, AD-associated inflammation renders this pathway dispensable. Instead, a previously unrecognized basophil-leukotriene (LT) axis emerges as critical for acute itch flares. By probing fundamental itch mechanisms, our study highlights a basophil-neuronal circuit that may underlie a variety of neuroimmune processes.

INTRODUCTION

Itch (i.e., pruritus) is defined as an uncomfortable sensation on the skin that causes a desire to scratch. When acute, itch is a protective mechanism to rapidly expel noxious environmental stimuli. However, itch can become chronic and pathologic in nature, underlying a variety of medical conditions that range from inflammatory skin disorders to chronic kidney disease and cancer (Larson et al., 2019; Sommer et al., 2007). Chronic itch is clinically defined in humans as itch that lasts for greater than 6 weeks (Kim et al., 2019; Ständer et al., 2017). Notably, chronic itch often persists for years due to the lack of effective therapeutics and can profoundly affect quality of life of patients (Altınok Ersoy and Akyar, 2019; Kini et al., 2011). In recent years, the morbidity of chronic itch has been increasingly recognized and clinical trials now routinely measure itch as a key endpoint (Fishbane et al., 2020; Kim et al., 2020a, 2020b; Silverberg et al., 2020; Ständer et al., 2020). However, current assessments quantify itch severity as an aggregate score over time (Erickson and Kim, 2019), despite the fact that patients with chronic itch often experience acute itch flares, i.e., rapid and intense exacerbations of itch (Fourzali et al., 2020; Langan et al., 2006). This results in

studies failing to assess the dynamic nature of itch in chronic conditions. Although substantial progress has been made in the identification of itch-specific neural pathways (Cevikbas et al., 2014; Liu et al., 2009, 2016; Mishra and Hoon, 2013; Oetjen et al., 2017; Sun and Chen, 2007; Wilson et al., 2013), the neuroimmune mechanisms that modulate itch acuity remain poorly defined.

Atopic dermatitis (AD) is a pruritic inflammatory skin disease with a chronic but relapsing course. Although chronic itch is a well-defined feature of AD, patients also report experiencing sudden itch flares, which remain poorly characterized (Chang et al., 2016; Fourzali et al., 2020; Wassmann-Otto et al., 2018). Recent advances in neuroimmunology have demonstrated that effector cytokines associated with AD such as interleukin-4 (IL-4), IL-13, and IL-31 can directly stimulate sensory neurons to promote chronic itch (Cevikbas et al., 2014; Oetjen et al., 2017). Whether acute itch flares simply represent enhanced signaling of these known pathways or use other molecular circuits remains unknown.

Characterized by scaly, leaky, and oozing skin, patients with AD become epicutaneously sensitized to environmental allergens and thus harbor allergen-specific immunoglobulin E (IgE) (Spergel and Paller, 2003; Weidinger et al., 2018). Although the acquisition of allergen-specific IgE predisposes patients with AD to develop other atopic disorders such as asthma and food allergy (Brough et al., 2015; Čelakovská et al., 2015; Flohr et al., 2014; Gustafsson et al., 2000), the role of IgE in AD pathogenesis has remained surprisingly elusive (Ogawa et al., 2016). Even in murine models of AD that are induced by model allergens, cutaneous inflammation occurs independently of IgE (Spergel et al., 1999). Furthermore, anti-IgE therapy has produced mixed results and has not advanced beyond phase 2 clinical trials in human AD, for which trial endpoints are primarily focused on skin inflammation and not itch (Deleanu and Nedelea, 2019; Heil et al., 2010). Nonetheless, several studies have demonstrated that patients with AD have seasonal variation of itch symptoms (Kim et al., 2017; Vocks et al., 2001) and exhibit enhanced itch following allergen exposure (Jaworek et al., 2020; Krämer et al., 2005; Werfel et al., 2015). Therefore, we hypothesized that IgE may represent a key mechanism that drives acute itch flares in response to allergens in the context of AD.

Residing in close proximity to sensory nerve fibers at barrier surfaces (Egan et al., 1998; Letourneau et al., 1996; Stead et al., 1987; Undem et al., 1995), mast cells are poised to rapidly respond to a variety of stimuli to orchestrate a multitude of physiologic processes (Benoist and Mathis, 2002; Galli and Tsai, 2012; Gupta and Harvima, 2018; Marshall, 2004; Voehringer, 2013). The most well-studied mechanism of mast cell activation is IgE-mediated degranulation. Allergen recognition by IgE bound to the high-affinity receptor FcεRI results in IgE crosslinking and triggers the release of a variety of effector molecules such as histamine and serotonin (Benditt et al., 1955; Ishizaka et al., 1970). These mediators in turn can activate sensory neurons to provoke neuroinflammation and itch sensation (Wang et al., 2020). Indeed, histamine was one of the first factors identified to elicit itch through its direct stimulation of sensory neurons (i.e., to act as a pruritogen), and it is now recognized as a canonical mediator of acute itch (Dale and Laidlaw, 1910; Weisshaar et al., 1997). However, antihistamines have demonstrated poor efficacy in most chronic itch disorders, including AD (He et al., 2018; Rajagopalan et al., 2017).

In the current study, we examined clinical itch datasets from phase 3 clinical trials for moderate-to-severe AD and found that a large proportion of patients exhibit acute itch flares that would not be captured in traditional analyses. Furthermore, we identified that patients with allergen-specific IgE have a higher likelihood of exhibiting acute itch flares than those without allergen-specific IgE, provoking the hypothesis that allergen exposure is a factor that drives acute itch flares. To investigate this, we generated a murine model of AD-like disease in which challenge with a model allergen elicits acute itch flares. Although dependent on IgE, acute itch flares surprisingly occurred independently of tissue-resident mast cells, but they were critically dependent on basophils. Strikingly, chemogenetic activation of basophils alone was sufficient to provoke itch-induced scratching behavior in mice. Intravital imaging further demonstrated basophil-sensory neuron interactions following cutaneous allergen exposure. Moreover, allergen-stimulated basophils exhibited enhanced production of leukotriene (LT) C4. The presence of cysteinyl LT receptor 2 (CysLTR2) on neurons, a receptor for LTC4, was critically required for acute itch flares in AD-associated inflammation. Collectively, our study unveils a form of acute itch flare that emerges in the context of chronic skin inflammation to activate a non-canonical basophil-neuronal circuit. Importantly, we highlight how itch manifests heterogeneously even within one disease.

RESULTS

Patients with AD exhibit acute itch flare patterns that are associated with allergen-specific IgE

Although patients suffering from chronic itch can experience acute periods of intense itch exacerbation (Fourzali et al., 2020; Langan et al., 2006), this phenomenon remains poorly characterized. To study AD-associated acute itch flares, we performed a post hoc analysis on two phase 3 clinical trials for moderate-to-severe AD (Simpson et al., 2016). We assessed the daily numerical rating scale (NRS) itch scores from placebo-treated patients (N = 159) over a 2-month period (Figure 1A). The NRS itch score is a single-item self-assessment wherein patients rate their severity of itch from 0 ("no itch") to 10 ("worst imaginable itch") over the prior 24 h (Phan et al., 2012). While some patients exhibited consistent itch severity over the assessment period, others exhibited a fluctuating itch pattern with rapid and frequent spikes of itch (Figure 1B). We classified patients as having an acute itch flare if there was an elevation in their daily NRS itch score of $\geq$2 points relative to their baseline (day 0) within a 3-day period (Langan et al., 2006). During the first month, 26.4% of the patients (42/159) exhibited acute itch flares (Figure 1C). In the second month, interestingly, N = 5 patients (5/159, 3.1%) lost their acute itch phenotype, while N = 32 patients (32/159, 20.1%), who previously exhibited a non-flare pattern, developed acute itch flares (Figure 1D). Overall, 46.5% of patients with AD (74/159) presented with acute itch flares during the course of the 2-month period (Figures 1C and 1D).

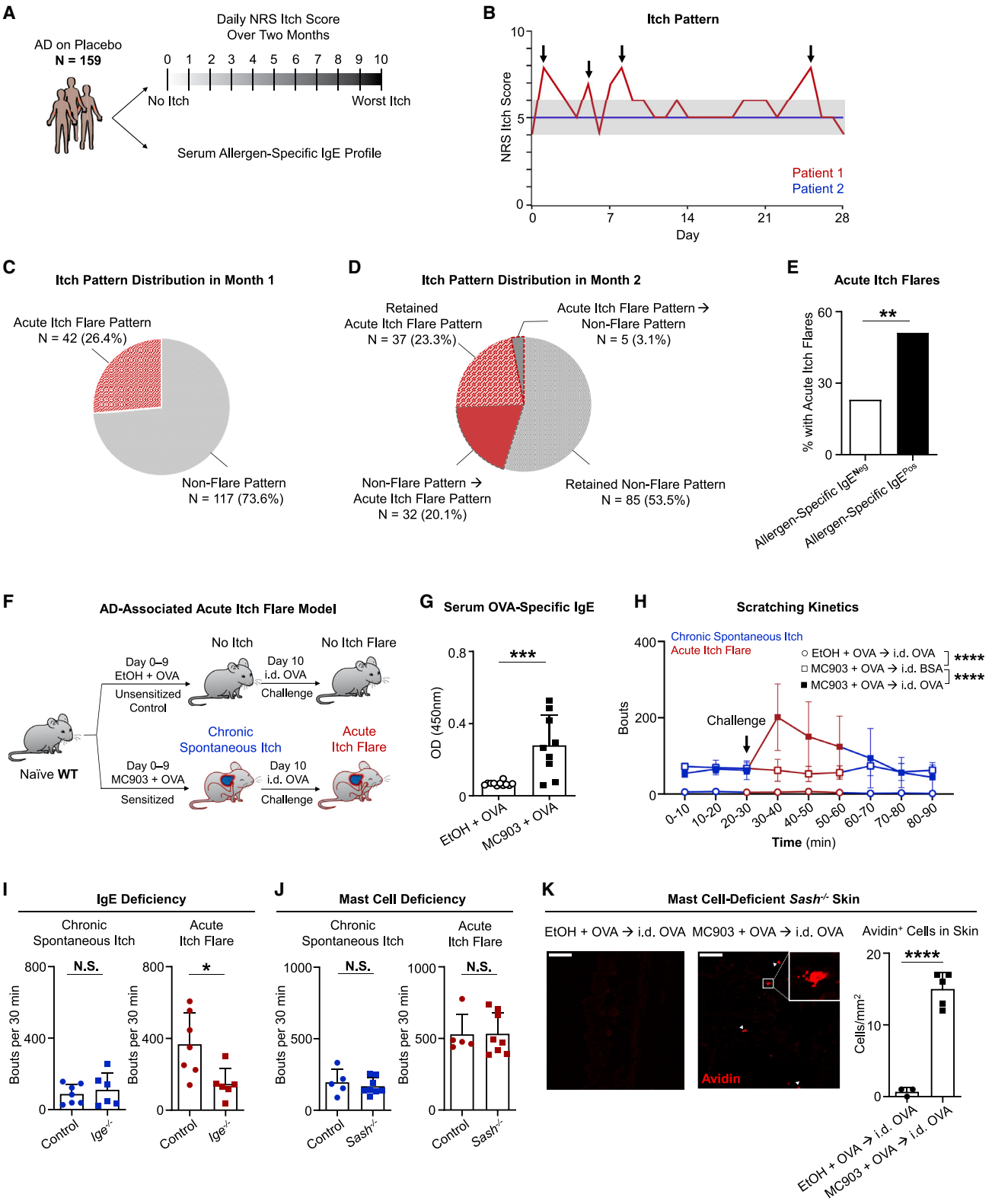

(legend on next page)

Collectively, our data demonstrate that acute itch flares are exhibited by a large proportion of patients with AD. However, what factors drive these periodic itch exacerbations remain unclear.

Prior studies have found that allergens provoke itch in AD (Jaworek et al., 2020; Krämer et al., 2005; Werfel et al., 2015). Furthermore, the majority of patients with AD harbor allergen-specific IgE (Flohr et al., 2004). To investigate whether reactivity to allergens is linked to acute itch flares, we retrospectively profiled the serum allergen-specific IgE repertoire from our cohort of N = 159 patients (Figure 1A). We separated patients into those who harbor allergen-specific IgE (N = 133 patients, 83.6%) and those who do not (N = 26 patients, 16.4%). Strikingly, a higher frequency of patients with allergen-specific IgE (68/133, 51.1%) experienced acute itch flares than those without allergen-specific IgE (6/26, 23.1%) (Figure 1E). Taken together, these findings indicate that the presence of allergen-specific IgE is likely associated with acute itch flares in AD, provoking the hypothesis that allergen exposure might be a factor that drives acute itch flares.

Acute itch flares are mast cell-independent in a murine model of AD-like disease

To test whether allergen recognition by IgE promotes acute itch flares in the setting of AD-associated inflammation, we generated a murine model of acute itch flares. We induced AD-like disease by topically treating mice on both ears with the irritant calcipotriol (MC903) daily for 10 days. Concurrently with MC903, the model allergen ovalbumin (OVA) was also topically applied onto the ear skin in order to mirror epicutaneous allergen sensitization (Figures 1F and S1A) that occurs in patients (Han et al., 2017; Noti et al., 2013). After 10 days, MC903 + OVA-treated wild-type (WT) mice developed robust AD-like skin inflammation (Figures S1B and S1C), allergen (OVA)-specific IgE (Figure 1G), and chronic spontaneous itch (~60 bouts/10 min) (Figure 1H, blue line, open and closed squares). This was in contrast to WT mice that received the control treatment of ethanol vehicle and OVA (EtOH + OVA), which lacked skin inflammation (Figures S1B and S1C), OVA-specific IgE (Figure 1G), and chronic spontaneous itch behavior (~5 bouts/10 min) over the same interval (Figure 1H, blue line, open circle). Upon intradermal (i.d.) injection of OVA into the adjacent non-lesional cheek skin of mice with AD-associated inflammation (Figure 1F), an acute itch flare was immediately observed (~200 bouts/10 min) and resolved over the subsequent 30 min (Figure 1H, red line, closed square). However, this acute itch flare phenomenon was absent in EtOH + OVA-treated control mice i.d. challenged with OVA (Figure 1H, red line, open circle) and in mice with AD-associated inflammation that were i.d. challenged with an irrelevant allergen, bovine serum albumin (BSA) (Figure 1H, red line, open square). As expected, IgE was required for acute itch flares as IgE-deficient (*Ige*$^{-/-}$) mice failed to generate a response to i.d. OVA challenge, while IgE was dispensable for chronic spontaneous itch (Figure 1I). These studies demonstrate that acute itch flares triggered by allergen exposure are dependent on IgE in the context of AD.

Mast cell degranulation induced by IgE crosslinking is well known to trigger acute itch sensation (Gould and Sutton, 2008; Meixiong et al., 2019). Indeed, when naive WT were passively sensitized by intravenous (i.v.) transfer of exogenous

Figure 1. Acute itch flares are associated with allergen-specific IgE in human AD and mast cell-independent in murine atopic dermatitis (AD)-like disease

(A) Schematic of post hoc analysis of phase 3 clinical trial data from a cohort of placebo-treated patients with AD (N = 159). For each patient, the daily numerical rating scale (NRS) itch scores over a 2-month period and the serum allergen-specific IgE repertoire were assessed.

(B) Itch patterns from two representative individuals. Patient 1 (red line) has an acute itch flare pattern due to the presence of at least one acute itch flare (indicated by arrows). Patient 2 (blue line) has a non-flare itch pattern due to a lack of apparent itch flares. Gray shading highlights 2-point threshold above baseline for patient 1.

(C) Pie chart depicting the percentage (%) of patients with an acute itch flare or non-flare pattern in the first month.

(D) Pie chart depicting the percentage (%) of patients with various itch patterns in month 2. Wedges outlined by dotted lines represent patients whose itch pattern changed from month 1 to month 2.

(E) Frequency of patients who exhibited acute itch flares over the 2-month observation period out of all patients that tested positive for allergen-specific IgE (black bar, N = 68/133) and out of all patients that tested negative (white bar, N = 6/26). **$p < 0.01$ by chi-square test.

(F) Schematic of the AD-associated acute itch flare model. Calcipotriol (MC903) + ovalbumin (OVA)-treated (sensitized; from day 0 to day 9) or ethanol (EtOH) + OVA-treated (unsensitized control; from day 0 to day 9) wild-type (WT) mice received an intradermal (i.d.) injection of OVA into adjacent non-lesional cheek skin on day 10. Prior to and following i.d. OVA challenge, chronic spontaneous itch and acute itch flares were recorded, respectively.

(G) ELISA quantification of OVA-specific IgE in the sera of MC903 + OVA-treated and EtOH + OVA-treated WT mice on day 10 of the AD-associated acute itch flare model. n = 9–11 mice per group. ***$p < 0.001$ by unpaired Student's t test.

(H) Number of scratching bouts in 10-min intervals prior to and following i.d. allergen (OVA or bovine serum albumin [BSA]) challenge on day 10 of the AD-associated acute itch flare model. Unsensitized (EtOH + OVA) mice were challenged with i.d. OVA (open circle), and sensitized (MC903 + OVA) mice were challenged with i.d. OVA (closed square) or i.d. BSA (open square). Blue line indicates chronic spontaneous itch, and red line indicates acute itch flares. n = 7 mice per group. ****$p < 0.0001$ by two-way ANOVA test.

(I) Number of scratching bouts in littermate control and *Ige*$^{-/-}$ mice prior to i.d. OVA challenge (chronic spontaneous itch; left) and following i.d. OVA challenge (acute itch flares; right) on day 10 of the AD-associated acute itch flare model. n = 6–7 mice per group. *$p < 0.05$ by unpaired Student's t test. N.S., not significant.

(J) Number of scratching bouts in littermate control and mast cell-deficient *Sash*$^{-/-}$ mice prior to i.d. OVA challenge (chronic spontaneous itch; left) and following i.d. OVA challenge (acute itch flares; right) on day 10 of the AD-associated acute itch flare model. n = 5–8 mice per group. N.S. by unpaired Student's t test.

(K) Representative images of i.d. OVA-challenged skin sections stained with avidin-Texas red (tetramethylrhodamine-isothiocyanate [TRITC]) in unsensitized (EtOH + OVA) or sensitized (MC903 + OVA) mast cell-deficient *Sash*$^{-/-}$ mice and the number of avidin-positive cells quantified per square millimeter from each treatment group. White arrows indicate positively stained cells. White square indicates zoomed view of an avidin-positive cell. n = 3–5 mice per group. ****$p < 0.0001$ by unpaired Student's t test. Scale bar, 50 μm.

Data are represented as mean ± SD.

See also Figure S1.

anti-OVA IgE and then challenged with i.d. OVA (Figure S1D), they experienced robust acute itch (Figure S1E) that was dependent on both mast cells (Figure S1F) and histamine (Figure S1G). Surprisingly, however, in our AD-associated acute itch flare model, both chronic spontaneous itch and acute itch flares were not significantly different between mast cell-deficient *Sash*$^{-/-}$ and littermate control mice (Figure 1J). To corroborate these observations using an alternative method of sensitization, we transferred anti-OVA IgE into MC903-treated WT mice or mast cell-deficient *Sash*$^{-/-}$ mice and subsequently challenged them with i.d. OVA to elicit acute itch flares (Figures S1H and S1I). Again, *Sash*$^{-/-}$ mice had comparable acute itch flares to their littermate controls in this setting (Figure S1J). Taken together, these findings demonstrate that allergen-provoked acute itch, while mast cell-dependent and histaminergic in the steady state, occurs independently of mast cells in the setting of AD-like disease. Thus, it appears that AD-associated inflammation activates an alternative IgE-dependent cellular circuit to evoke acute itch flares. In support of this, cells with a distinctly degranulated morphology as identified by avidin staining (Bergstresser et al., 1984; Mukai et al., 2017) were evident in MC903 + OVA-treated mast cell-deficient *Sash*$^{-/-}$ mice at the site of i.d. OVA challenge (Figure 1K), indicating the presence of an alternative cell type.

Circulating basophils exhibit a distinct phenotype in AD-associated inflammation in mice and humans

Basophils, like tissue-resident mast cells, also express the high-affinity IgE receptor FcεRI and release similar effector molecules such as histamine, serotonin, tryptase, and LTs following IgE crosslinking (Voehringer, 2013). Despite their importance in driving cutaneous inflammation and their functional similarities to mast cells (Borriello et al., 2014; Ito et al., 2011; Kim et al., 2014a; Mashiko et al., 2017; Mukai et al., 2005), the role of basophils in itch remains unknown. Given that basophils are not skin resident, but rather circulate in the blood and enter the skin upon stimulation, we sought to investigate whether AD-associated inflammation systemically alters basophils.

To test this, we performed flow cytometry on the blood of patients with AD (N = 12) and healthy control subjects (N = 12) (Figure 2A; Table S1). Strikingly, AD-associated blood basophils, although unchanged in frequency (Figure 2B), exhibited elevated expression of the human basophil marker CD203c (Figure 2C). Cytokines such as IL-3 upregulate CD203c expression on human basophils and enhance IgE-mediated responses (Brunner et al., 1993). In support of the possibility that AD-associated basophils may be more reactive to IgE stimulation, blood basophils from patients with AD demonstrated significantly enhanced expression of FcεRIα compared with basophils from control subjects (Figure 2D). Similarly, mice with AD-like disease (Figures 2E and S2A) did not display differences in the frequency of circulating basophils (Figure 2F). Instead, they exhibited rapid and sustained upregulation of the murine basophil activation marker CD200R (Figures 2G and S2B) and FcεRIα compared with control mice (Figures 2H and S2C). These findings provoke the hypothesis that basophils are more responsive to IgE-mediated stimulation, which may enable their ability to promote itch.

Chemogenetic activation of basophils is sufficient to elicit itch

We next asked whether direct activation of basophils alone is sufficient to induce acute itch. To test this, we used a chemogenetic approach by crossing the basophil-specific *Mcpt8*-Cre-YFP (yellow fluorescent protein) mouse with the Rosa26-LSL-Gq-DREADD (designer receptors exclusively activated by designer drugs) line. The resulting *Mcpt8*-Gq mice have a targeted insertion of the artificial G protein-coupled receptor (GPCR) hM3Dq into basophils, allowing for selective activation upon administration of an otherwise inert compound, clozapine-*N*-oxide (CNO) (Figure 3A). To confirm this, we obtained sort-purified blood basophils from *Mctp8*-Gq mice and littermate controls and stimulated them *ex vivo* with CNO. As expected, basophils from *Mctp8*-Gq mice displayed enhanced degranulation compared with littermate controls (Figures 3B–3D). We then assessed itch behavior following systemic intraperitoneal (i.p.) administration of CNO to *Mcpt8*-Gq mice. Strikingly, *Mcpt8*-Gq mice exhibited markedly enhanced scratching following CNO injection compared with littermate control mice (Figure 3E). These findings demonstrate that basophil activation alone is sufficient to evoke itch behavior.

Basophils are required for acute itch flares in AD-associated inflammation

Next, we tested whether basophils are required to mediate acute itch flares in the context of AD-associated inflammation. We depleted basophils with systemic anti-CD200R3 monoclonal antibody (mAb) administration on day 7 and day 9 of the AD-associated acute itch flare model (Figure 4A). Basophil depletion (Figure 4B) significantly decreased the acute itch flare response to i.d. OVA challenge (Figure 4C). We next used an alternative approach by utilizing Bas-TRECK mice, which exclusively express the diphtheria toxin (DT) receptor on basophils (Figure 4D) (Noti et al., 2013). Genetic depletion of basophils with i.p. DT administration on day 8 and day 9 of the AD-associated acute itch flare model (Figure 4E) resulted in reduced scratching in response to i.d. OVA challenge (Figure 4F). Moreover, neither endogenous OVA-specific IgE production nor the underlying chronic spontaneous itch behavior was affected by basophil depletion with either anti-CD200R3 mAb treatment (Figure S3A) or in Bas-TRECK mice (Figure S3B). Therefore, our data demonstrate that basophils are critically required in promoting acute itch flares in the setting of AD-associated inflammation. Furthermore, to test the specificity of the contribution of basophils to acute itch flares, we used an alternative method of OVA sensitization whereby mice were systemically sensitized by i.p. injection of OVA along with the adjuvant alum (Figure S3C) (Huang et al., 2016; Meixiong et al., 2019). In the context of systemic sensitization, acute itch was indeed observed in WT mice following i.d. OVA challenge (Figure S3D). However, in this context, acute itch was attenuated in mast cell-deficient *Sash*$^{-/-}$ mice (Figure S3E), but not in basophil-depleted Bas-TRECK mice (Figure S3F). Strikingly, upon induction of AD-like disease by MC903 along with systemic sensitization with i.p. OVA + alum (Figure S3G), allergen-provoked acute itch flares were unaffected in mast cell-deficient *Sash*$^{-/-}$ mice (Figure S3H) but significantly attenuated in basophil-depleted Bas-TRECK mice (Figure S3I).

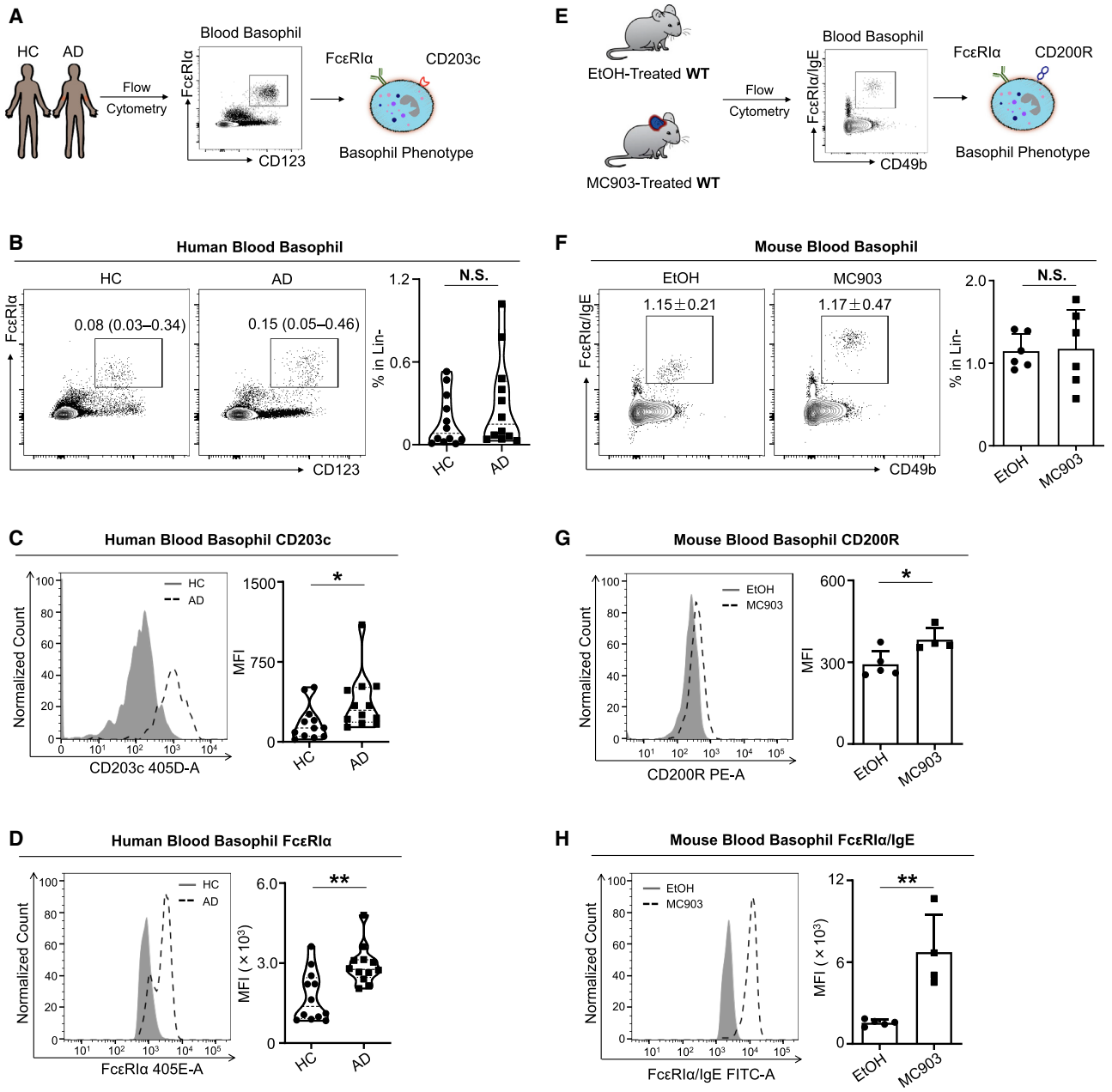

Figure 2. Circulating basophils exhibit a distinct phenotype in AD-associated inflammation in mice and humans

(A) Schematic of human blood basophil analysis by flow cytometry from healthy controls (HCs) and patients with AD.

(B) Representative flow cytometry plots and frequency of lineage negative (Lin^-) (CD3, CD4, CD19, CD14, CD34, CD56, c-Kit) $CD123^+$ $Fc\varepsilon RI\alpha^+$ blood basophils from HCs and patients with AD. N = 12 subjects per group. N.S. by Wilcoxon-Mann-Whitney nonparametric test.

(C and D) CD203c (C) and FcεRIα (D) expression measured by mean fluorescence intensity (MFI) on blood basophils from HCs and patients with AD. N = 12 subjects per group. *$p < 0.05$, **$p < 0.01$ by Wilcoxon-Mann-Whitney nonparametric test.

(E) Schematic of murine blood basophil analysis by flow cytometry. Vehicle EtOH or MC903 was topically applied on the ear skin of WT mice from day 0 to day 9 to induce AD-like disease.

(F) Representative flow cytometry plots and frequency of Lin^- (CD3e, CD5, CD11c, CD19, NK1.1) $CD49b^+$ $Fc\varepsilon RI\alpha/IgE^+$ blood basophils in EtOH- or MC903-treated WT mice on day 10 of the AD-like disease model. n = 6 mice per group. N.S. by unpaired Student's t test.

(G and H) CD200R (G) and FcεRIα/IgE (H) expression measured by MFI on blood basophils in EtOH- or MC903-treated WT mice on day 10 of the AD-like disease model. n = 4–5 mice per group. *$p < 0.05$, **$p < 0.01$ by unpaired Student's t test.

Data are represented as median (interquartile range) in (B)–(D) and mean ± SD in (F)–(H).

See also Figure S2 and Table S1.

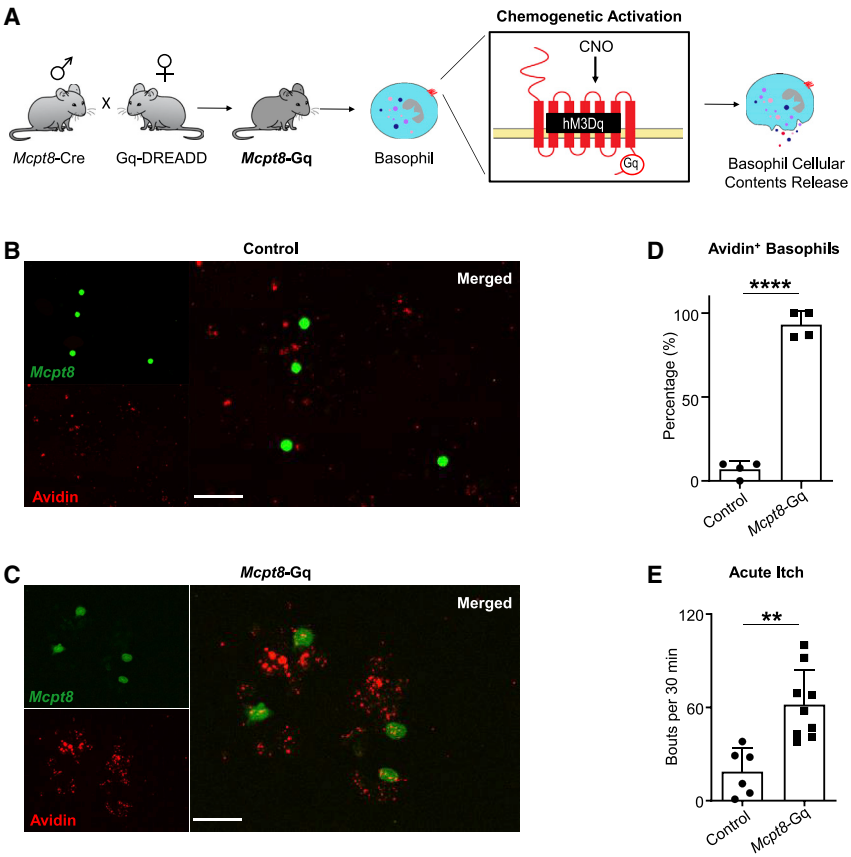

Figure 3. Chemogenetic activation of basophils is sufficient to elicit itch

(A) Schematic of the *Mcpt8*-Gq mouse line. Generated by crossing the Cre-dependent Gq-DREADD line with the *Mcpt8*-Cre-YFP line, *Mcpt8*-Gq mice specifically express hM3Dq in basophils allowing for selective chemogenetic activation of basophils upon clozapine-*N*-oxide (CNO) administration.

(B and C) Representative images of basophils isolated from the blood of (B) control (*Mcpt8*-Cre) or (C) *Mcpt8*-Gq mice that were stimulated *ex vivo* with CNO. Identified based on their expression of the YFP reporter (fluorescein isothiocyanate [FITC], green), basophils were additionally stained with avidin-Texas red (TRITC, red). Scale bar, 50 μm.

(D) Frequency of blood basophils isolated from control (*Mcpt8*-Cre) and *Mcpt8*-Gq mice that were avidin positive following *ex vivo* stimulation with CNO. n = 4 mice per group. ****$p < 0.0001$ by unpaired Student's t test.

(E) Number of scratching bouts following intraperitoneal (i.p.) injection of CNO in control (*Mcpt8*-Cre) and *Mcpt8*-Gq mice. n = 6–9 mice per group. **$p < 0.01$ by unpaired Student's t test.

Data are represented as mean ± SD.

Taken together, these results indicate that the contribution of basophils to acute itch flares arises in the context of AD-like inflammation rather than other forms of sensitization (i.e., OVA + alum).

Mast cells release a number of mediators that directly stimulate sensory neurons to modify sensory behavior (Voehringer, 2013). We thus hypothesized that factors derived from allergen-stimulated basophils are sufficient to provoke acute itch behavior. To test this, we first purified blood basophils from sensitized (MC903 + OVA) and unsensitized (EtOH + OVA) WT mice and stimulated them *ex vivo* with OVA (Figure 4G). We then i.d. injected supernatants into naive WT recipient mice to determine their ability to induce acute itch (Figure 4H). Strikingly, basophil-derived factors from sensitized mice induced robust scratching not observed with supernatants from unsensitized mice (Figure 4I). We next sought to test whether basophil-derived factors can directly stimulate primary sensory neurons. We isolated dorsal root ganglia (DRG) from *Pirt*$^{GCaMP3/+}$ calcium reporter mice (Kim et al., 2014b) and tested whether different factors could activate primary sensory neurons by calcium imaging. We first validated that sensory neurons were not responsive to OVA stimulation alone (Figures S3J and S3K). We then added basophil-derived supernatants from both unsensitized (EtOH + OVA) and sensitized (MC903 + OVA) WT mice to DRG neurons (Figure 4J). Notably, enhanced calcium responses were detected in sensory neurons stimulated with supernatants from allergen-sensitized basophils compared with supernatants from unsensitized basophils (Figures 4K and 4L). Additionally, the subpopulation of sensory neurons responsive to basophil-derived factors was also activated by capsaicin (Figure 4K), a common feature of many itch-sensory or pruriceptive neurons (Dong and Dong, 2018). Overall, these findings demonstrate that factors derived from basophils can induce acute itch and activate sensory neurons.

Acute itch flares require basophil-intrinsic LT pathways

Next, we investigated the specific effector mechanisms by which basophils promote acute itch flares in AD-like disease. The most well-defined pruritogens associated with mast cells include histamine, serotonin, tryptase, and LTs (Akiyama et al., 2010; Andoh and Kuraishi, 1998; Meixiong et al., 2019; Solinski et al., 2019). To determine whether any of these pathways are enriched in basophils, we analyzed publicly available microarray datasets to specifically compare murine blood basophils to skin-resident mast cells (Benoist et al., 2012; Dwyer et al., 2016). Skin mast cells expressed higher levels of *Hdc* (histidine decarboxylase, the primary enzyme catalyzing histamine synthesis), *Tph1* (tryptophan hydroxylase [TPH] 1, which controls peripheral serotonin synthesis), and *Tpsab1* (tryptase) compared with blood basophils (Figures 5A–5C). By contrast, blood basophils expressed higher levels of *Alox5ap* (Figure 5D), which encodes arachidonate 5-lipoxygenase-activating protein, also known as 5-lipoxygenase-activating protein (FLAP) (Mancini et al., 1993). LT biosynthesis is critically controlled by the key enzyme 5-lipoxygenase (5-LOX), which requires FLAP for activation (Hedi and Norbert, 2004). Therefore, we hypothesized that LT biosynthesis is a key pathway underlying acute itch flares. In support of this, antihistamines (Figure 5E), an inhibitor of serotonin production

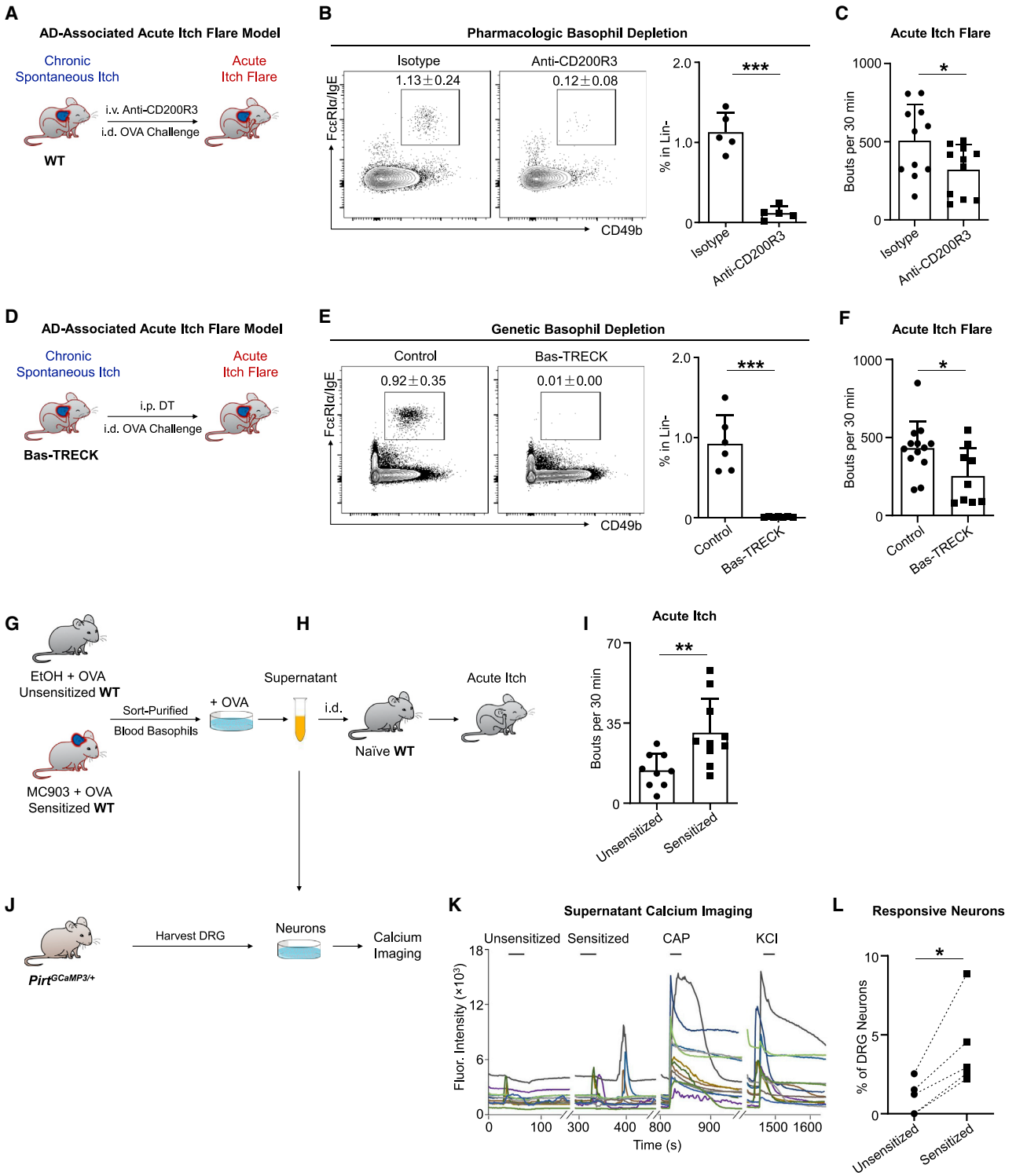

Figure 4. Basophils are required for acute itch flares in AD-associated inflammation

(A) Schematic of pharmacologic basophil depletion. WT mice received intravenous (i.v.) injection of isotype control or anti-CD200R3 monoclonal antibody (mAb) on day 7 and day 9 of the AD-associated acute itch flare model (MC903 + OVA).

(B) Representative flow cytometry plots and frequency of Lin$^-$ (CD3e, CD5, CD11c, CD19, NK1.1) FcεRIα/IgE$^+$ CD49b$^+$ basophils from the blood of isotype-treated and anti-CD200R3 mAb-treated WT mice prior to i.d. OVA challenge on day 10 of the AD-associated acute itch flare model. n = 5 mice per group. ***$p < 0.001$ by unpaired Student's t test.

(legend continued on next page)

(Figure 5F), and an antagonist of the tryptase receptor protease-activated receptor 2 (PAR2) (Figure 5G) were all ineffective in attenuating allergen-provoked acute itch flares during AD-associated inflammation. By contrast, pharmacologic inhibition of 5-LOX by zileuton or genetic deficiency of 5-LOX (*Alox5*$^{-/-}$ mice) markedly and significantly reduced acute itch flares (Figure 5H). Additionally, disruption of the 5-LOX pathway did not affect the quantity of allergen-specific IgE (Figure S4A) or the levels of chronic spontaneous itch (Figure S4B). Collectively, these results indicate that LTs may mediate acute itch flares.

We then tested whether LTs released from basophils mediate allergen-provoked acute itch flares. We obtained sort-purified basophils from sensitized (MC903 + OVA) *Alox5*$^{-/-}$ or littermate control mice (Figure 5I), stimulated them *ex vivo* with OVA, and then i.d. injected the respective basophil-derived supernatants into naive WT recipient mice. Indeed, supernatants derived from *Alox5*$^{-/-}$ basophils did not evoke acute itch behavior like supernatants from littermate control basophils (Figure 5J). To exclude the role of LTs released from mast cells, we topically treated mast cell-deficient *Sash*$^{-/-}$ mice with MC903 + OVA and then gave them an oral gavage of the 5-LOX inhibitor zileuton or vehicle control prior to i.d. OVA challenge (Figure 5K). Pharmacologic inhibition of 5-LOX attenuated acute itch flares (Figure 5L), indicating that the effect of LT inhibition is independent of mast cells. By contrast, zileuton treatment of basophil-deficient Bas-TRECK mice was not able to additionally suppress acute itch flares (Figures 5M and 5N), demonstrating that basophils selectively mediate the induction of acute itch flares via LTs. Taken together, our data implicate basophil-derived LTs as key inducers of allergen-provoked acute itch flares in AD-associated inflammation.

Basophils interact with sensory neurons in the skin upon allergen challenge

Because of the close proximity of mast cells to nerves in the skin and their capacity to evoke histaminergic itch, the mast cell-nerve unit has classically represented a central neuroimmune axis in itch (Gupta and Harvima, 2018; Wang et al., 2020). Having found that factors derived from allergen-activated basophils can directly activate sensory neurons *in vitro*, we next sought to visualize whether basophils interact with cutaneous sensory neurons *in vivo*. Although rare in circulation, basophils can rapidly migrate in response to various stimuli such as cytokines and IgE stimulation (Hirsch and Kalbfleisch, 1980; Lett-Brown et al., 1981; Suzukawa et al., 2005) and thereby infiltrate tissues (Egawa et al., 2013; Hellman et al., 2017; Ito et al., 2011; Min et al., 2004; Voehringer, 2017; Wardlaw et al., 1994). Therefore, we hypothesized that stimulation of basophils with allergen in the skin may result in unique basophil-neuronal interactions that could support their role in itch.

To test this, we used *Mcpt8*-Cre-YFP mice in which YFP is specifically expressed on basophils, but not on mast cells (Sullivan et al., 2011; Voehringer, 2013). We subjected *Mcpt8*-Cre-YFP reporter mice to our AD-associated acute itch flare model and performed real-time intravital two-photon imaging to visualize allergen-challenged skin (Figure 6A). In unsensitized (EtOH + OVA) control mice, no basophils were observed in the skin before or after i.d. OVA challenge (Figure 6B). However, in the skin of sensitized (MC903 + OVA) mice, basophils were detected in the dermis but were primarily non-motile with a round morphology (Figure 6B; Video S1). Strikingly, after i.d. OVA challenge, the majority of basophils developed an enlarged, elongated morphology and began to crawl through the dermis (Figure 6B; Video S2). Collectively, these findings demonstrate that in the setting of AD-associated inflammation, basophils alter their shape and increase their patrolling behavior in response to allergen challenge.

To examine whether basophils can acquire the ability to interact with sensory neurons *in vivo*, we generated bone marrow chimeric mice by transferring bone marrow cells from *Mcpt8*-Cre-YFP donors into irradiated sensory neuron reporter ($Na_V1.8$-TdTomato) mice (Figure 6C). Intravital two-photon imaging confirmed the presence of round and immotile basophils

(C) Number of scratching bouts following i.d. OVA challenge on day 10 of the AD-associated acute itch flare model in isotype-treated WT mice and basophil-depleted (anti-CD200R3 mAb-treated) WT mice. n = 11 mice per group. *$p < 0.05$ by unpaired Student's t test.

(D) Schematic of conditional basophil depletion by i.p. injection of diphtheria toxin (DT) into Bas-TRECK mice on day 8 and day 9 of the AD-associated acute itch flare model.

(E) Representative flow cytometry plots and frequency of Lin$^-$ (CD3e, CD5, CD11c, CD19, NK1.1) FcεRIα/IgE$^+$ CD49b$^+$ basophils from the blood of littermate control and Bas-TRECK mice prior to i.d. OVA challenge on day 10 of the AD-associated acute itch flare model. n = 6–7 mice per group. ***$p < 0.001$ by unpaired Student's t test.

(F) Number of scratching bouts following i.d. OVA challenge on day 10 of the AD-associated acute itch flare model in littermate control and basophil-depleted Bas-TRECK mice. n = 9–13 mice per group. *$p < 0.05$ by unpaired Student's t test.

(G) Schematic of sort purification and culture of circulating basophils from unsensitized (EtOH + OVA) or sensitized (MC903 + OVA) WT mice. Supernatants were collected 1 h following *ex vivo* stimulation with OVA.

(H) Schematic of i.d. injection of supernatants from OVA-stimulated basophils (from Figure 4G) into naive WT mice to test acute itch responses.

(I) Number of scratching bouts in naive WT recipient mice following i.d. injection of basophil-derived supernatants from unsensitized (EtOH + OVA) or sensitized (MC903 + OVA) WT mice. n = 9–10 recipient mice per group. **$p < 0.01$ by unpaired Student's t test.

(J) Schematic of dorsal root ganglia (DRG) neurons isolated from *Pirt*$^{GCaMP3/+}$ calcium reporter mice being stimulated with supernatants from OVA-stimulated basophils (from Figure 4G) to test calcium responses using calcium imaging.

(K) Representative calcium traces of mouse DRG responses to supernatant stimulation. Calcium responses were measured by fluorescence (Fluor.) intensity (488 nm). Neurons isolated from *Pirt*$^{GCaMP3/+}$ mice were sequentially stimulated with supernatants from unsensitized (EtOH + OVA) mice, supernatants from sensitized (MC903 + OVA) mice, capsaicin (CAP; 500 nM), and KCl (50 mM). Each color trace represents one neuron.

(L) Percentage (%) of supernatant-responsive neurons out of all KCl-responsive neurons. Each data point represents the percent of supernatant-responsive neurons from one individual *Pirt*$^{GCaMP3/+}$ mouse. n = 5 mice (>200 neurons each). *$p < 0.05$ by paired Student's t test.

Data are represented as mean ± SD.

See also Figure S3.

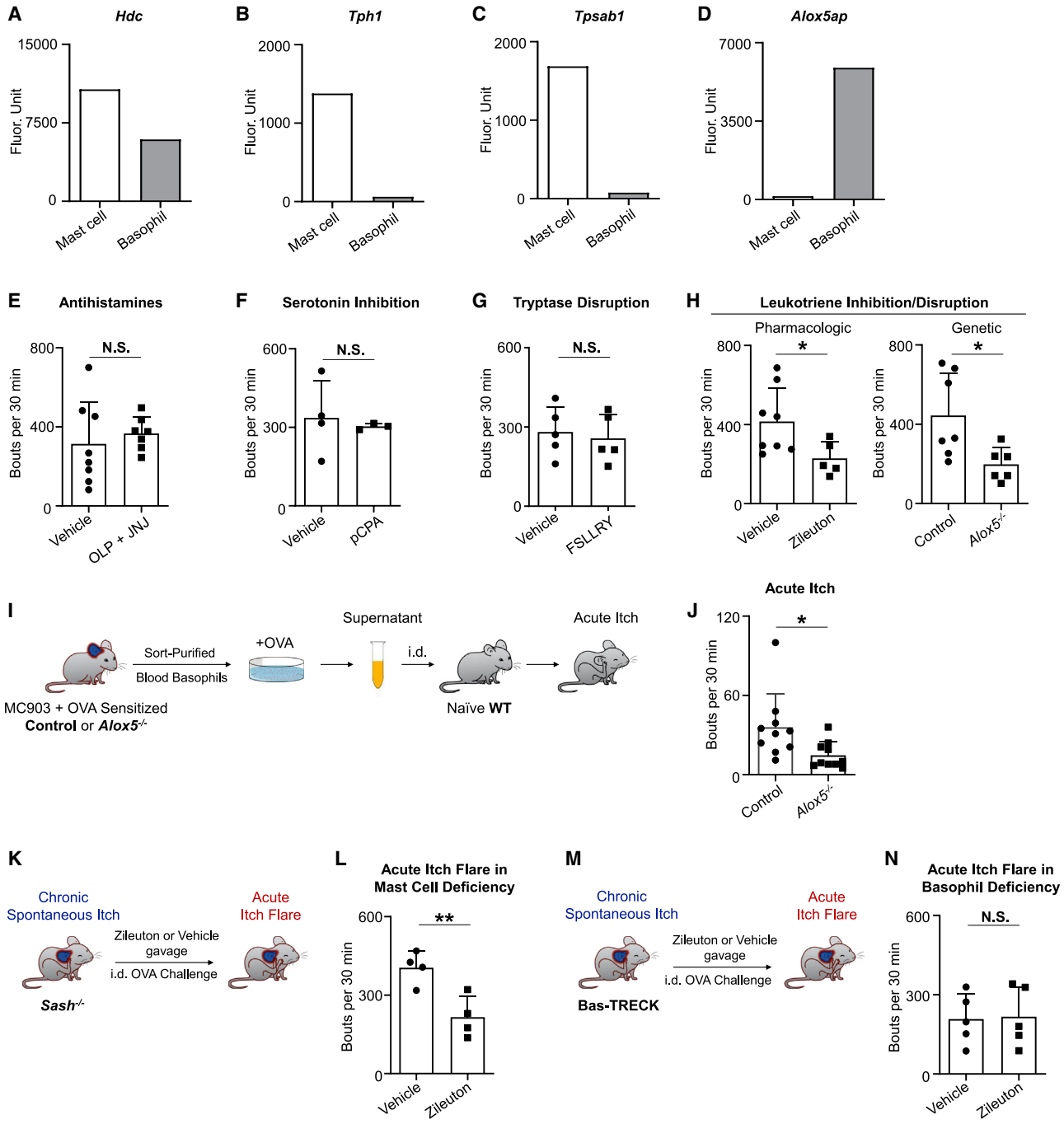

Figure 5. Acute itch flares require basophil-intrinsic leukotriene (LT) pathways

(A–D) RNA expression of (A) *Hdc*, (B) *Tph1*, (C) *Tpsab1*, and (D) *Alox5ap* in murine skin mast cells and blood basophils. Raw data from www.immgen.org.

(E) Number of scratching bouts following i.d. OVA challenge on day 10 of the AD-associated acute itch flare model in WT mice that were pre-administered vehicle or antihistamines olopatadine (OLP; 3 mg/kg i.p.) and JNJ7777120 (JNJ; 20 mg/kg subcutaneous injection into the nape) 30 min prior to i.d. OVA challenge. n = 7–8 mice per group. N.S. by unpaired Student's t test.

(F) Number of scratching bouts following i.d. OVA challenge on day 10 of the AD-associated acute itch flare model in WT mice that were pre-administered vehicle or tryptophan hydroxylase inhibitor *p*-chlorophenylalanine (pCPA; 150 mg/kg i.p.) on day 7, day 8, and day 9. n = 3–4 mice per group. N.S. by unpaired Student's t test.

(G) Number of scratching bouts following i.d. OVA challenge on day 10 of the AD-associated acute itch flare model in WT mice that were pre-administered vehicle or protease-activated receptor 2 (PAR2, the tryptase receptor) antagonist FSLLRY-NH_2 (FSLLRY, 7.5 mg/kg i.p.) 30 min prior to i.d. OVA challenge. n = 5 mice per group. N.S. by unpaired Student's t test.

(legend continued on next page)

in the skin of sensitized (MC903 + OVA) chimeric mice prior to allergen challenge (Figure 6D; Video S3). As observed previously, allergen (OVA) challenge rapidly induced basophil motility with track speeds ranging from 2 to 6 μm/min (Figure 6E; Video S4) and polarized morphology (Figure 6F) consistent with a migratory phenotype (Rappel and Edelstein-Keshet, 2017). Strikingly, the motile basophils were seen migrating through the dermis and making frequent and extended apparent contacts with sensory nerve fibers (Figures 6D, 6G, and 6H; Video S5). Taken together, these data demonstrate that basophils are capable of directly interacting with sensory nerve fibers in the skin.

The LTC4-CysLTR2 neuroimmune axis underlies acute itch flares

Given that basophils interact with sensory neurons and are a significant source of LTs, we sought to investigate the neuronal mechanisms by which LTs promote acute itch flares. Generated from arachidonic acid via the 5-LOX pathway, LTs are a diverse family comprised of LTA4, LTB4, LTC4, LTD4, and LTE4 (Luster and Tager, 2004; Schauberger et al., 2016). LTB4 and LTC4 have previously been shown to function as pruritogens in mice (Andoh and Kuraishi, 1998; Fernandes et al., 2013; Solinski et al., 2019). To determine which LT likely mediates allergen-provoked acute itch flares, we measured serum LTB4 and LTC4 levels in sensitized (MC903 + OVA) WT mice challenged with i.d. OVA or BSA. Strikingly, in contrast to LTB4 (Figure 7A), higher levels of LTC4 were detected in mice challenged with i.d. OVA than in mice challenged with i.d. BSA (Figure 7B). In addition, when we obtained sort-purified basophils from sensitized (MC903 + OVA) and unsensitized (EtOH + OVA) WT mice and stimulated them *ex vivo* with OVA, we found elevated LTC4 production from sensitized basophils compared with unsensitized basophils (Figure 7C). More importantly, basophil-depleted Bas-TRECK mice exhibited lower serum LTC4 levels than littermate controls following i.d. OVA challenge in the AD-associated acute itch flare model (Figure 7D). Collectively, these data suggest that LTC4 upregulation is dependent on basophils and could be a key pruritogen in allergen-evoked acute itch flares.

Because LTC4 can be converted to LTD4 and metabolized, we used a non-metabolizable form of LTC4, *N*-methyl LTC4 (N-met LTC4) and confirmed that i.d. injection induces robust scratching behavior in naive WT mice (Figure 7E). Indeed, dose-response analysis comparing N-met LTC4 to histamine indicates that N-met LTC4 is a more potent pruritogen (Figure 7F). LTC4 has two receptors, CysLTR1 and CysLTR2, both of which are broadly expressed in multiple tissues. However, CysLTR2 is also expressed on sensory neurons (Sasaki and Yokomizo, 2019). To explore which sensory neurons may be responsive to LTC4, we mined a single-cell RNA sequencing (scRNA-seq) database of mouse DRG (Usoskin et al., 2015). Three putative clusters of itch-sensory neurons have been codified by transcriptional profiling: non-peptidergic (NP) 1, NP2, and NP3. CysLTR2 is predominantly and selectively expressed by NP3 neurons (Figure S5A) (Solinski et al., 2019; Usoskin et al., 2015). By performing calcium imaging, we found that ~12% of DRG neurons responded to N-met LTC4, which almost exclusively overlapped with serotonin-responsive NP3 neurons, but not β-alanine-responsive NP1 or chloroquine-responsive NP2 neurons (Figures S5B and S5C). Therefore, we sought to investigate whether blockade of CysLTR2 signaling could ameliorate acute itch flares in AD-like disease. Indeed, systemic CysLTR2 blockade with the antagonist HAMI3379 (Figure 7G) significantly and specifically reduced allergen-provoked itch flares in sensitized (MC903 + OVA) WT mice (Figures 7H and S6A), while systemic disruption of the LTB4 pathway or CysLTR1 pathway had no effect (Figures S6B and S6C). Furthermore, we sought to test whether disruption of CysLTR2 on neurons would be sufficient to reduce acute itch flares. We performed small interfering RNA (siRNA) *in vivo* delivery via intracisternal injection to knockdown the expression of CysLTR2 at the neuronal level (Figure 7I) (Li et al., 2019; Liu et al., 2011). Compared with control siRNA, delivery of CysLTR2 siRNA resulted in notable knockdown of CysLTR2 protein as determined by immunofluorescence of sensory trigeminal ganglia (Figure 7J). Importantly, siRNA knockdown of CysLTR2 also significantly and selectively inhibited acute itch flares (Figures 7K and S6D). These results indicate that the LTC4-CysLTR2 axis is critical for the pathogenesis of acute itch flares.

The downstream signaling events of CysLTR2 on sensory neurons remain poorly understood. The majority of newly identified itch receptors are GPCRs that depend on various downstream transient receptor potential (TRP) cation channels for their

(H) Number of scratching bouts following i.d. OVA challenge on day 10 of the AD-associated acute itch flare model in WT mice that were pre-administered vehicle or zileuton (a 5-lipoxygenase [5-LOX] inhibitor, 50 mg/kg by gavage) 60 min prior to i.d. OVA challenge (left). Number of scratching bouts following i.d. OVA challenge on day 10 of the AD-associated acute itch flare model in littermate control and *Alox5*$^{-/-}$ mice (right). n = 5–8 mice per group. *$p < 0.05$ by unpaired Student's t test.

(I) Schematic for testing the pruritogenic properties of circulating basophils from sensitized (MC903 + OVA) littermate control or *Alox5*$^{-/-}$ mice stimulated *ex vivo* with OVA. Supernatants suspended from stimulated basophils were i.d. injected into naive WT mice to provoke acute itch responses.

(J) Number of scratching bouts in naive WT recipient mice i.d. injected with basophil-derived supernatants from sensitized littermate control or sensitized *Alox5*$^{-/-}$ mice. n = 10 recipient mice per group. *$p < 0.05$ by unpaired Student's t test.

(K) Schematic for testing the 5-LOX pathway in mast cell-deficient *Sash*$^{-/-}$ mice pre-administered vehicle or zileuton prior to i.d. OVA challenge on day 10 of the AD-associated acute itch flare model.

(L) Number of scratching bouts following i.d. OVA challenge on day 10 of the AD-associated acute itch flare model in mast cell-deficient *Sash*$^{-/-}$ mice that were pre-administered vehicle or zileuton (50 mg/kg by gavage). n = 4 mice per group. **$p < 0.01$ by unpaired Student's t test.

(M) Schematic for testing 5-LOX pathway in basophil-depleted Bas-TRECK mice pre-administered vehicle or zileuton prior to i.d. OVA challenge on day 10 of the AD-associated acute itch flare model.

(N) Number of scratching bouts following i.d. OVA challenge on day 10 of the AD-associated acute itch flare model in basophil-depleted Bas-TRECK mice that were pre-administered vehicle or zileuton (50 mg/kg by gavage). n = 5 mice per group. N.S. by unpaired Student's t test.

Data are represented as mean ± SD.

See also Figure S4.

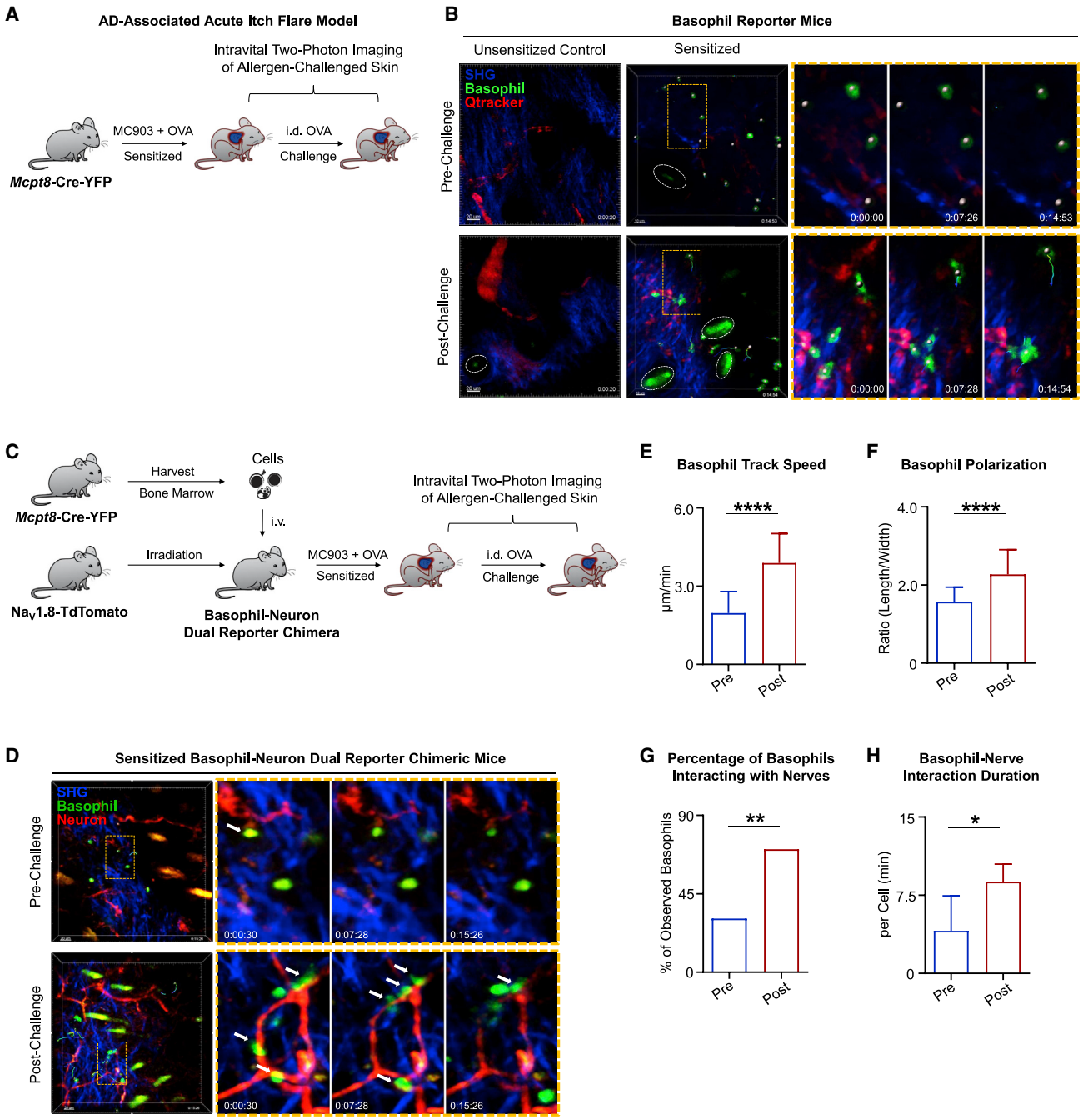

Figure 6. Basophils interact with sensory neurons in the skin upon allergen challenge

(A) Schematic of intravital two-photon imaging of cheek skin (injection site) pre- and post-challenge with i.d. OVA in *Mcpt8*-Cre-YFP mice on day 10 of the AD-associated acute itch flare model.

(B) Time-lapse intravital two-photon imaging of basophil behavior. Representative images were taken of the cheek skin from unsensitized (EtOH + OVA) control and sensitized (MC903 + OVA) *Mcpt8*-Cre-YFP mice, pre- and post-challenge with i.d. OVA. Tracked basophils (green) are indicated by white dots (center of mass). Autofluorescent hairs are identified by white ellipses. Basophil motility is indicated by time-encoded colored tracks. Zoomed views are taken from the regions outlined by orange rectangles. Blood vessels (red) were labeled by i.v. injection of Qtracker 655 vascular label 15–30 min prior to imaging. Collagen (blue) is imaged by collecting the second harmonic generation signal (SGH).

(C) Schematic of basophil-neuron dual reporter chimera generation and intravital two-photon imaging of the cheek skin (injection site) in sensitized (MC903 + OVA) dual reporter mice pre- and post-challenge with i.d. OVA on day 10 of the AD-associated acute itch flare model. Bone marrow cells harvested from *Mcpt8*-Cre-YFP donors were i.v. injected into $Na_V1.8$-TdTomato recipients after X-ray irradiation to generate dual reporter mice. Mice were rested 8 weeks before initiation of AD-associated acute itch flare model.

(legend continued on next page)

function (Sun and Dong, 2016; Veldhuis et al., 2015). Thus, we hypothesized that CysLTR2, also a GPCR (Evans, 2002), would require TRP signaling for its function in sensory neurons. Using calcium imaging, we found that the N-met LTC4-responsive neurons almost entirely overlap with neurons that respond to both the TRPV1 agonist capsaicin and the TRPA1 agonist allyl isothiocyanate (AITC) (Figures 7L and 7M). However, genetic deletion of *Trpv1* or *Trpa1* alone was not sufficient to block N-met LTC4-mediated calcium responses (Figure 7N). We then used compound *Trpv1* and *Trpa1* double-deficient mice (Feng et al., 2017) and found that dual deletion abolished calcium responses in sensory neurons (Figure 7N). These findings mirror our *in vivo* results that N-met LTC4-induced scratching behavior was unaffected in either *Trpv1*$^{-/-}$ or *Trpa1*$^{-/-}$ mice compared with their respective littermate controls (Figures S7A and S7B). By contrast, *Trpv1*$^{-/-}$ *Trpa1*$^{-/-}$ mice exhibited significant reduction in itch behavior in response to N-met LTC4 (Figure 7O). Similar to N-met LTC4 injection, *Trpv1*$^{-/-}$ *Trpa1*$^{-/-}$ mice exhibited a reduction in OVA-mediated acute itch flares (Figure 7P), while having no effect on the underlying chronic spontaneous itch (Figure S7C). Collectively, we demonstrate that acute itch flares in the inflammatory state use the LTC4-CysLTR2 pathway, which can utilize either TRPV1 or TRPA1 to promote itch signaling in sensory neurons.

DISCUSSION

Atopy is defined as a predisposition to allergen hypersensitivity and enhanced IgE production (Coca and Cooke, 1923; Justiz Vaillant and Jan, 2020). The family of atopic diseases includes AD, allergic rhinitis, asthma, and food allergy. Despite being a canonical atopic disorder, the role of IgE in AD remains surprisingly unclear. Indeed, clinical trials with anti-IgE mAb (omalizumab) have been met with mixed results in AD (Deleanu and Nedelea, 2019). Our study suggests, however, that IgE is critical not for chronic itch development but for promoting acute itch flares. Thus, the failures of these clinical trials may have been due to an inability to capture the rapid and dynamic changes in itch by routine clinical assessments. Our high-resolution analysis of phase 3 clinical trial data uncovered that a larger proportion of patients with AD exhibit acute itch flares than previously recognized. Furthermore, we found that the presence of allergen-specific IgE in patients with AD may predispose them to the development of acute itch flares. Thus, our findings demonstrate that heterogeneous forms of itch with unique underlying mechanisms can co-exist within one chronic condition.

Basophils have been suggested to induce pruritus due to their expression of a multitude of pruritogens such as histamine and type 2 cytokines (Steinhoff et al., 2018). However, this has remained unstudied. Thus, we undertook a chemogenetic gain-of-function approach to demonstrate that selective activation of basophils alone is sufficient to induce itch in mice. Although basophils critically promote AD-like skin inflammation (Imai et al., 2019; Kim et al., 2014a; Walsh et al., 2019), surprisingly, we found that they do not mediate chronic spontaneous itch. Furthermore, our study reveals that while mast cells and histamine are critical for acute itch in the steady state, basophils and LTC4 mediate acute itch flares in AD-like disease. Thus, our findings provide insight into the long-standing controversy about the role of mast cells and histamine in atopy and unveil a role for basophils in mediating itch.

Although our study shows that both mast cells and basophils can induce itch in response to the same allergen, in the setting of AD-associated inflammation, basophils emerge as the key effector cell. It is well known that cytokines such as IL-3 can prime basophils to become more reactive to IgE stimulation (Brunner et al., 1993). Indeed, we found that both murine and human basophils upregulate FcεRIα in the setting of AD-associated inflammation. Taken together, these findings suggest that AD-associated inflammation enhances the capacity of basophils to mediate allergen-induced itch. While our current study focused on IgE-dependent itch, we speculate that basophils may use other mechanisms as well to promote itch in other settings. Indeed, in mast cells, two distinct itch-promoting pathways have recently emerged: (1) histaminergic, IgE-dependent itch and (2) non-histaminergic, Mas-related GPCR (Mrgpr) B2-dependent itch (Meixiong et al., 2019). Recent studies have shown that the human ortholog of MrgprB2, MRGPRX2, is expressed on human basophils (Wedi et al., 2020). Thus, future studies will be required to understand the precise role of MRGPRs and other GPCRs on basophils and their potential role in itch.

(D) Time-lapse intravital two-photon imaging of basophil-neuron interactions in the cheek skin of basophil-neuron dual reporter chimeric mice, pre- and post-challenge with i.d. OVA on day 10 of the AD-associated acute itch flare model. Representative images show sensory nerve fibers (red) and basophils (green, white dots). Tracked cell motility is shown as time-encoded colored tracks. Autofluorescent hairs appear yellow or green and collagen appears blue due to the SHG signal. Zoomed views are taken from the regions outlined by orange rectangles. White arrows show examples of basophils making apparent contacts with sensory nerves in the skin.

(E) Basophil track speed in the cheek skin of basophil-neuron dual reporter chimeric mice, pre- and post-challenge with i.d. OVA on day 10 of the AD-associated acute itch flare model. n > 20 basophils per group. Data are represented as median (interquartile range). ****$p < 0.0001$ by Wilcoxon-Mann-Whitney nonparametric test. n = 3 mice.

(F) Basophil polarization (length/width ratio) in the cheek skin of basophil-neuron dual reporter chimeric mice, pre- and post-challenge with i.d. OVA on day 10 of the AD-associated acute itch flare model. n > 20 basophils per group. ****$p < 0.0001$ by unpaired Student's t test. n = 3 mice.

(G) Percentage (%) of basophils interacting with nerve fibers in the cheek skin of basophil-neuron dual reporter chimeric mice, pre- and post-challenge with i.d. OVA on day 10 of the AD-associated acute itch flare model. n > 20 basophils per group. **$p < 0.01$ by chi-square test. n = 3 mice.

(H) Basophil-nerve interaction durations normalized to cell number of basophils in the skin of basophil-neuron dual reporter chimeric mice, pre- and post-challenge with i.d. OVA on day 10 of the AD-associated acute itch flare model. n > 20 observed basophils per group. *$p < 0.05$ by unpaired Student's t test. n = 3 mice.

Data are represented as mean ± SD in (F) and (H).

See also Videos S1, S2, S3, S4, and S5.

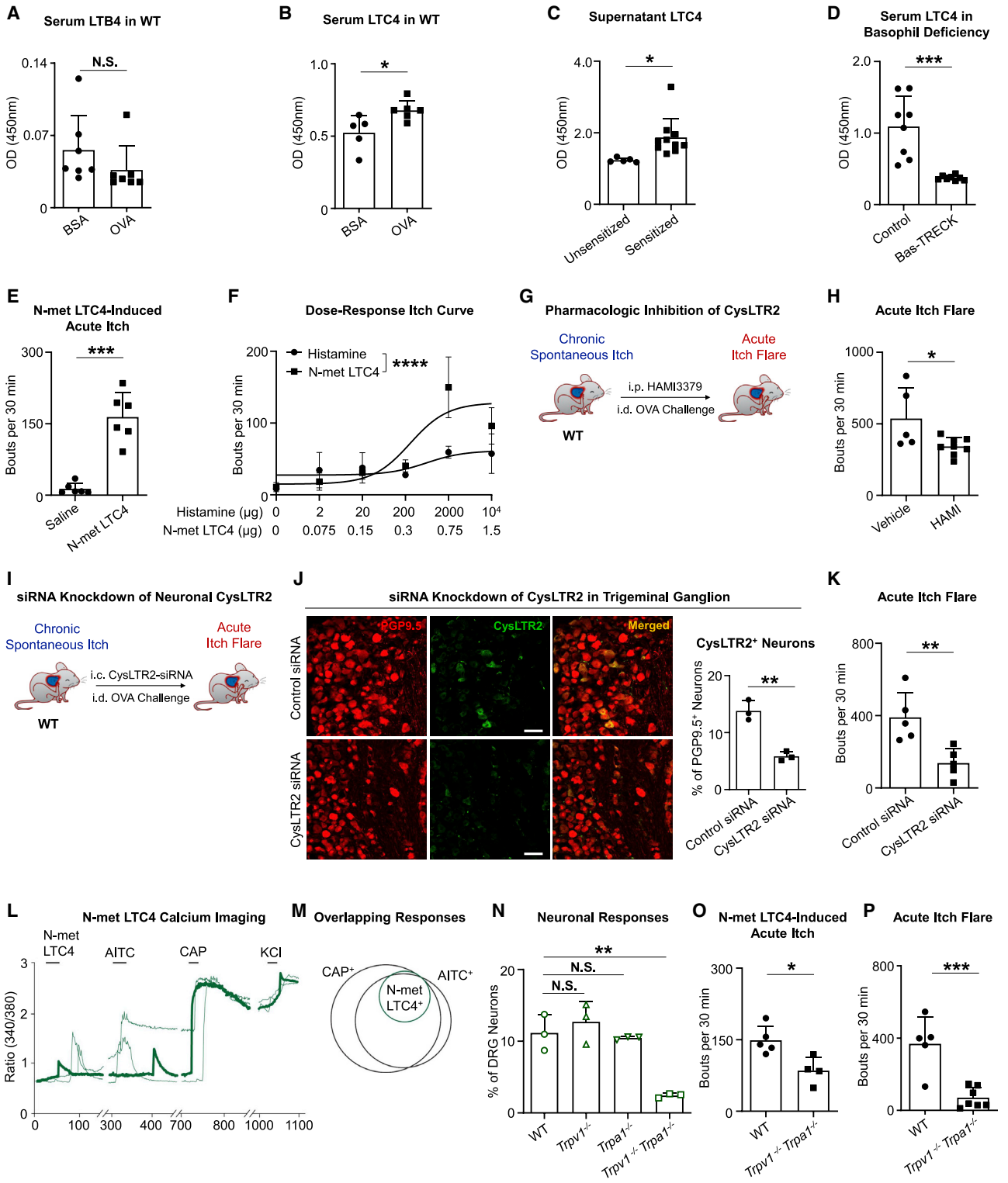

Figure 7. The LTC4-CysLTR2 axis underlies acute itch flares

(A) ELISA quantification of serum LTB4 levels in sensitized (MC903 + OVA) WT mice challenged with i.d. BSA or OVA on day 10 of the AD-associated acute itch flare model. n = 7 mice per group. N.S. by unpaired Student's t test.

(legend continued on next page)

A striking observation in our study was that LTC4 almost exclusively activated a subpopulation of sensory neurons referred to as NP3. Interestingly, the receptor for IL-31 (*Il31ra*) is exclusively expressed on the NP3 population (Usoskin et al., 2015). The first cytokine to be identified as a pruritogen (Cevikbas et al., 2014), therapies targeting IL-31 pathway such as nemolizumab are rapidly advancing in clinical trials for AD and other chronic itch disorders (Kabashima et al., 2018; Ruzicka et al., 2017; Ständer et al., 2020). Recent studies suggest that human basophils may be a cellular source of IL-31 (Raap et al., 2017). Whether basophil-derived IL-31 may synergize with LTC4 to amplify acute itch flares in AD remains to be determined. Collectively, these findings demonstrate that basophils activate a subpopulation of sensory neurons that is strongly associated with inflammatory itch.

It is widely appreciated that mast cells are tissue resident in nature and mediate a variety of homeostatic neuroimmune processes such as vasoregulation, neuroinflammation, and sensation due to their close proximity with neurons (Gupta and Harvima, 2018; Voehringer, 2013). By contrast, basophils are circulating and generally not present in tissues in the steady state. However, under pathologic conditions, basophils can be rapidly recruited into inflamed tissue (Miyake and Karasuyama, 2017). Thus, we speculate that basophils are more likely to be proinflammatory in nature and underlie maladaptive neuroimmune processes. Our study provides additional evidence of evolutionarily distinct roles between mast cells and basophils in both health and disease.

STAR★METHODS

Detailed methods are provided in the online version of this paper and include the following:

- KEY RESOURCES TABLE
- RESOURCE AVAILABILITY
  - Lead contact
  - Materials availability
  - Data and code availability
- EXPERIMENTAL MODEL AND SUBJECT DETAILS
  - Human subjects
  - Research animals
- METHOD DETAILS
  - Mouse model
  - Skin inflammation assessment and histopathology
  - Pharmacologic treatments administration in mouse models
  - Behavioral tests
  - ELISA
  - Flow cytometry

(B) ELISA quantification of serum LTC4 levels in sensitized (MC903 + OVA) WT mice challenged with i.d. BSA or OVA on day 10 of the AD-associated acute itch flare model. n = 5–6 mice per group. *$p < 0.05$ by unpaired Student's t test.

(C) ELISA quantification of LTC4 levels in supernatants collected from basophils stimulated *ex vivo* with OVA from unsensitized (EtOH + OVA) or sensitized (MC903 + OVA) WT mice (as in Figure 4G). n = 5–10 mice per group. *$p < 0.05$ by unpaired Student's t test.

(D) ELISA quantification of serum LTC4 levels in sensitized (MC903 + OVA) littermate control and basophil-depleted Bas-TRECK mice challenged with i.d. OVA on day 10 of the AD-associated acute itch flare model. n = 8 mice per group. ***$p < 0.001$ by unpaired Student's t test.

(E) Number of scratching bouts following i.d. injection of saline or *N*-methyl LTC4 (N-met LTC4, 0.75 μg) in WT mice. n = 6 mice per group. ***$p < 0.001$ by unpaired Student's t test.

(F) Dose-response curves of scratching bouts quantified in WT mice following i.d. challenge with increasing doses of histamine (0–10,000 μg) or N-met LTC4 (0–1.5 μg). n ≥ 3 mice per dosage in each group. ****$p < 0.0001$ by two-way ANOVA test.

(G) Schematic for pharmacologic inhibition of CysLTR2 in WT mice pre-administered vehicle or HAMI3379 (HAMI) prior to i.d. OVA challenge on day 10 of the AD-associated acute itch flare model.

(H) Number of scratching bouts following i.d. OVA challenge on day 10 of the AD-associated acute itch flare model in WT mice that were pre-administered vehicle or CysLTR2 antagonist HAMI (0.4 mg/kg i.p.) on day 9 (two doses) and on day 10 (one dose, 60 min prior to challenge). n = 5–8 mice per group. *$p < 0.05$ by unpaired Student's t test.

(I) Schematic for neuronal CysLTR2 inhibition in WT mice pretreated with daily intracisternal (i.c.) injection of control siRNA or CysLTR2 siRNA from day 7 to day 9 followed by i.d. OVA challenge on day 10 of the AD-associated acute itch flare model.

(J) Representative images of the trigeminal ganglion stained with PGP9.5 (TRITC, red) and CysLTR2 (FITC, green) and the percentage (%) of CysLTR2-positive cells out of all PGP9.5-positive neurons in sensitized (MC903 + OVA) WT mice that were pretreated with i.c. control siRNA or CysLTR2 siRNA. n = 3 mice per group. **$p < 0.01$ by unpaired Student's t test. Scale bar, 50 μm.

(K) Number of scratching bouts following i.d. OVA challenge on day 10 of the AD-associated acute itch flare model in WT mice that were pretreated with i.c. control siRNA or CysLTR2 siRNA. n = 5 mice per group. **$p < 0.01$ by unpaired Student's t test.

(L) Representative calcium traces of mouse sensory neuron responses to N-met LTC4 stimulation. Calcium levels were measured as a ratio of 340/380 nm fluorescence over time. DRG neurons isolated from WT mice were sequentially stimulated with N-met LTC4 (100 nM), allyl isothiocyanate (AITC, 100 μM), CAP (500 nM), and KCl (50 mM). Each trace represents one neuron.

(M) Representative Venn diagram depicting the overlapping responses of DRG neuron subsets to N-met LTC4 (100 nM), AITC (100 μM), and CAP (500 nM). n > 200 neurons from a WT mouse.

(N) Percentage (%) of N-met LTC4-responsive neurons out of all KCl-responsive neurons. DRG neurons were isolated from WT, *Trpv1*$^{-/-}$, *Trpa1*$^{-/-}$, or compound *Trpv1*$^{-/-}$ *Trpa1*$^{-/-}$ mice. Each data point represents the percent of neurons that were responsive to N-met LTC4 in an individual mouse. n = 3 mice (>200 neurons each) per group. N.S. and **$p < 0.01$ by unpaired Student's t test.

(O) Number of scratching bouts following i.d. injection of N-met LTC4 in WT (control) and compound *Trpv1*$^{-/-}$ *Trpa1*$^{-/-}$ mice. n = 4–5 mice per group. *$p < 0.05$ by unpaired Student's t test.

(P) Number of scratching bouts following i.d. OVA challenge on day 10 of the AD-associated acute itch flare model in WT (control) and compound *Trpv1*$^{-/-}$ *Trpa1*$^{-/-}$ mice. n = 5–7 mice per group. ***$p < 0.001$ by unpaired Student's t test.

Data are represented as mean ± SD.

See also Figures S5, S6, and S7.

- Immunofluorescence staining
- Basophil *in vivo* chemogenetic activation
- Basophil *in vivo* depletion
- Basophil sorting and cultures
- DRG neuronal cultures
- Calcium imaging of mouse DRG neurons
- Bone marrow transplant
- Two-photon microscopy
- Preparation and intracisternal injection of siRNA

● QUANTIFICATION AND STATISTICAL ANALYSIS

SUPPLEMENTAL INFORMATION

Supplemental Information can be found online at https://doi.org/10.1016/j.cell.2020.12.033.

ACKNOWLEDGMENTS

We thank Diane Bender and the Immunomonitoring Lab (IML) at the Andrew M. and Jane M. Burksy Center for Human Immunology & Immunotherapy Programs (ChiiPs). We also thank the In Vivo Imaging Core (IVIC) at the Washington University School of Medicine for their support of the intravital two-photon imaging studies. The Kim Lab is supported by NIAMS grants (K08-AR065577 and R01-AR070116), the American Skin Association, Doris Duke Charitable Foundation (to B.S.K.), and LEO Pharma. D.J.M. is supported by NIAMS grants (R01-AR060962 and R01-AR070873). M.J.M. is supported by NIAID grant (R01-AI077600). A.M.T. and M.R.M. were supported by NIAID training grant T32-AI716339. A.M.T. was also supported by the NIAID NRSA grant F30 AI154912. T.-L.B.Y. was supported by the Dermatology Foundation Dermatologist Investigator Research Fellowship (DIRF). The IML is a shared resource of the Alvin J. Siteman Cancer Center and is supported by the Andrew M. and Jane M. Bursky ChiiPs and NCI Cancer Center support grant (P30CA91842).

AUTHOR CONTRIBUTIONS

F.W. and B.S.K. designed the experiments. F.W. performed the experiments and analyzed the data. F.L. contributed to calcium imaging and siRNA delivery. Z.X. and X.D. assisted with calcium imaging. S.K. and M.J.M. performed two-photon imaging and did imaging data analyses. Z.C., J.D.H., and M.A. provided human data of itch scores and assisted the analyses. D.J.M. provided human blood samples and clinical assessments of control subjects and patients with AD. M.R.M., J.N.C., and C.S.H. assisted with flow cytometry. M.R.M. contributed to the graphical abstract. A.M.T., J.B., A.Z.X., and S.A.M. assisted with behavioral assays. X.D., H.H., Q.L., and M.K. donated mice. F.W., A.M.T., T.-L.B.Y., A.M.V.H., and B.S.K. wrote the manuscript. B.S.K. supervised the project.

DECLARATION OF INTERESTS

B.S.K. has served as a consultant for AbbVie, ABRAX Japan, Almirall, AstraZeneca, Cara Therapeutics, Daewoong Pharmaceutical, Incyte, LEO Pharma, Lilly, Maruho, Menlo Therapeutics, OM Pharma, Pfizer, and Third Rock Ventures. He has also participated on the advisory board for Almirall, Boehringer Ingelheim, Cara Therapeutics, Kiniksa Pharmaceuticals, Menlo Therapeutics, Regeneron Pharmaceuticals, Sanofi Genzyme, and Trevi Therapeutics. He is stockholder of Locus Biosciences. All other authors declare that they have no relevant conflicts of interest.

Received: May 21, 2020
Revised: October 9, 2020
Accepted: December 21, 2020
Published: January 14, 2021

REFERENCES

Akiyama, T., Carstens, M.I., and Carstens, E. (2010). Facial injections of pruritogens and algogens excite partly overlapping populations of primary and second-order trigeminal neurons in mice. J. Neurophysiol. *104*, 2442–2450.

Altınok Ersoy, N., and Akyar, İ. (2019). Multidimensional pruritus assessment in hemodialysis patients. BMC Nephrol. *20*, 42.

Andoh, T., and Kuraishi, Y. (1998). Intradermal leukotriene B4, but not prostaglandin E2, induces itch-associated responses in mice. Eur. J. Pharmacol. *353*, 93–96.

Benditt, E.P., Wong, R.L., Arase, M., and Roeper, E. (1955). 5-Hydroxytryptamine in mast cells. Proc. Soc. Exp. Biol. Med. *90*, 303–304.

Benoist, C., and Mathis, D. (2002). Mast cells in autoimmune disease. Nature *420*, 875–878.

Benoist, C., Lanier, L., Merad, M., and Mathis, D.; Immunological Genome Project (2012). Consortium biology in immunology: the perspective from the Immunological Genome Project. Nat. Rev. Immunol. *12*, 734–740.

Bergstresser, P.R., Tigelaar, R.E., and Tharp, M.D. (1984). Conjugated avidin identifies cutaneous rodent and human mast cells. J. Invest. Dermatol. *83*, 214–218.

Borriello, F., Granata, F., and Marone, G. (2014). Basophils and skin disorders. J. Invest. Dermatol. *134*, 1202–1210.

Brough, H.A., Liu, A.H., Sicherer, S., Makinson, K., Douiri, A., Brown, S.J., Stephens, A.C., Irwin McLean, W.H., Turcanu, V., Wood, R.A., et al. (2015). Atopic dermatitis increases the effect of exposure to peanut antigen in dust on peanut sensitization and likely peanut allergy. J. Allergy Clin. Immunol. *135*, 164–170.

Brunner, T., Heusser, C.H., and Dahinden, C.A. (1993). Human peripheral blood basophils primed by interleukin 3 (IL-3) produce IL-4 in response to immunoglobulin E receptor stimulation. J. Exp. Med. *177*, 605–611.

Čelakovská, J., Ettlerová, K., Ettler, K., Vaněčková, J., and Bukač, J. (2015). Sensitization to aeroallergens in atopic dermatitis patients: association with concomitant allergic diseases. J. Eur. Acad. Dermatol. Venereol. *29*, 1500–1505.

Cevikbas, F., Wang, X., Akiyama, T., Kempkes, C., Savinko, T., Antal, A., Kukova, G., Buhl, T., Ikoma, A., Buddenkotte, J., et al. (2014). A sensory neuron-expressed IL-31 receptor mediates T helper cell-dependent itch: Involvement of TRPV1 and TRPA1. J. Allergy Clin. Immunol. *133*, 448–460.

Chang, A., Robison, R., Cai, M., and Singh, A.M. (2016). Natural History of Food-Triggered Atopic Dermatitis and Development of Immediate Reactions in Children. J. Allergy Clin. Immunol. Pract. *4*, 229, 36.e1.

Charman, C.R., Venn, A.J., Ravenscroft, J.C., and Williams, H.C. (2013). Translating Patient-Oriented Eczema Measure (POEM) scores into clinical practice by suggesting severity strata derived using anchor-based methods. Br. J. Dermatol. *169*, 1326–1332.

Coca, A.F., and Cooke, R.A. (1923). On the classification of the phenomena of hypersensitiveness. J. Immunol. *8*, 163–182.

Dale, H.H., and Laidlaw, P.P. (1910). The physiological action of beta-iminazolylethylamine. J. Physiol. *41*, 318–344.

Deleanu, D., and Nedelea, I. (2019). Biological therapies for atopic dermatitis: An update. Exp. Ther. Med. *17*, 1061–1067.

Dong, X., and Dong, X. (2018). Peripheral and Central Mechanisms of Itch. Neuron *98*, 482–494.

Dwyer, D.F., Barrett, N.A., and Austen, K.F.; Immunological Genome Project Consortium (2016). Expression profiling of constitutive mast cells reveals a unique identity within the immune system. Nat. Immunol. *17*, 878–887.

Egan, C.L., Viglione-Schneck, M.J., Walsh, L.J., Green, B., Trojanowski, J.Q., Whitaker-Menezes, D., and Murphy, G.F. (1998). Characterization of unmyelinated axons uniting epidermal and dermal immune cells in primate and murine skin. J. Cutan. Pathol. *25*, 20–29.

Egawa, M., Mukai, K., Yoshikawa, S., Iki, M., Mukaida, N., Kawano, Y., Minegishi, Y., and Karasuyama, H. (2013). Inflammatory monocytes recruited to

allergic skin acquire an anti-inflammatory M2 phenotype via basophil-derived interleukin-4. Immunity *38*, 570–580.

Erickson, S., and Kim, B.S. (2019). Research Techniques Made Simple: Itch Measurement in Clinical Trials. J. Invest. Dermatol. *139*, 264–269.e1.

Evans, J.F. (2002). Cysteinyl leukotriene receptors. Prostaglandins Other Lipid Mediat. *68-69*, 587–597.

Feng, J., Yang, P., Mack, M.R., Dryn, D., Luo, J., Gong, X., Liu, S., Oetjen, L.K., Zholos, A.V., Mei, Z., et al. (2017). Sensory TRP channels contribute differentially to skin inflammation and persistent itch. Nat. Commun. *8*, 980.

Fernandes, E.S., Vong, C.T., Quek, S., Cheong, J., Awal, S., Gentry, C., Aubdool, A.A., Liang, L., Bodkin, J.V., Bevan, S., et al. (2013). Superoxide generation and leukocyte accumulation: key elements in the mediation of leukotriene B_4-induced itch by transient receptor potential ankyrin 1 and transient receptor potential vanilloid 1. FASEB J. *27*, 1664–1673.

Fishbane, S., Jamal, A., Munera, C., Wen, W., and Menzaghi, F.; KALM-1 Trial Investigators (2020). A Phase 3 Trial of Difelikefalin in Hemodialysis Patients with Pruritus. N. Engl. J. Med. *382*, 222–232.

Flohr, C., Johansson, S.G., Wahlgren, C.F., and Williams, H. (2004). How atopic is atopic dermatitis? J. Allergy Clin. Immunol. *114*, 150–158.

Flohr, C., Perkin, M., Logan, K., Marrs, T., Radulovic, S., Campbell, L.E., MacCallum, S.F., McLean, W.H.I., and Lack, G. (2014). Atopic dermatitis and disease severity are the main risk factors for food sensitization in exclusively breastfed infants. J. Invest. Dermatol. *134*, 345–350.

Fourzali, K.M., Golpanian, R.S., Chan, Y.H., and Yosipovitch, G. (2020). Average daily itch vs. worst daily itch in chronic itch evaluation. Br. J. Dermatol. *183*, 957–958.

Galli, S.J., and Tsai, M. (2012). IgE and mast cells in allergic disease. Nat. Med. *18*, 693–704.

Gould, H.J., and Sutton, B.J. (2008). IgE in allergy and asthma today. Nat. Rev. Immunol. *8*, 205–217.

Gupta, K., and Harvima, I.T. (2018). Mast cell-neural interactions contribute to pain and itch. Immunol. Rev. *282*, 168–187.

Gustafsson, D., Sjöberg, O., and Foucard, T. (2000). Development of allergies and asthma in infants and young children with atopic dermatitis–a prospective follow-up to 7 years of age. Allergy *55*, 240–245.

Han, H., Roan, F., and Ziegler, S.F. (2017). The atopic march: current insights into skin barrier dysfunction and epithelial cell-derived cytokines. Immunol. Rev. *278*, 116–130.

He, A., Feldman, S.R., and Fleischer, A.B., Jr. (2018). An assessment of the use of antihistamines in the management of atopic dermatitis. J. Am. Acad. Dermatol. *79*, 92–96.

Hedi, H., and Norbert, G. (2004). 5-Lipoxygenase Pathway, Dendritic Cells, and Adaptive Immunity. J. Biomed. Biotechnol. *2004*, 99–105.

Heil, P.M., Maurer, D., Klein, B., Hultsch, T., and Stingl, G. (2010). Omalizumab therapy in atopic dermatitis: depletion of IgE does not improve the clinical course - a randomized, placebo-controlled and double blind pilot study. J. Dtsch. Dermatol. Ges. *8*, 990–998.

Hellman, L.T., Akula, S., Thorpe, M., and Fu, Z. (2017). Tracing the Origins of IgE, Mast Cells, and Allergies by Studies of Wild Animals. Front. Immunol. *8*, 1749.

Hirsch, S.R., and Kalbfleisch, J.H. (1980). Existence of basophil chemotaxis in subjects with hay fever. J. Allergy Clin. Immunol. *65*, 274–277.

Huang, C.C., Kim, Y.S., Olson, W.P., Li, F., Guo, C., Luo, W., Huang, A.J.W., and Liu, Q. (2016). A histamine-independent itch pathway is required for allergic ocular itch. J. Allergy Clin. Immunol. *137*, 1267–1270.e6.

Huang, C.C., Yang, W., Guo, C., Jiang, H., Li, F., Xiao, M., Davidson, S., Yu, G., Duan, B., Huang, T., et al. (2018). Anatomical and functional dichotomy of ocular itch and pain. Nat. Med. *24*, 1268–1276.

Hussain, M., Borcard, L., Walsh, K.P., Pena Rodriguez, M., Mueller, C., Kim, B.S., Kubo, M., Artis, D., and Noti, M. (2018). Basophil-derived IL-4 promotes epicutaneous antigen sensitization concomitant with the development of food allergy. J. Allergy Clin. Immunol. *141*, 223–234.e5.

Imai, Y., Yasuda, K., Nagai, M., Kusakabe, M., Kubo, M., Nakanishi, K., and Yamanishi, K. (2019). IL-33-Induced Atopic Dermatitis-Like Inflammation in Mice Is Mediated by Group 2 Innate Lymphoid Cells in Concert with Basophils. J. Invest. Dermatol. *139*, 2185–2194.e3.

Ishizaka, K., Tomioka, H., and Ishizaka, T. (1970). Mechanisms of passive sensitization. I. Presence of IgE and IgG molecules on human leukocytes. J. Immunol. *105*, 1459–1467.

Ito, Y., Satoh, T., Takayama, K., Miyagishi, C., Walls, A.F., and Yokozeki, H. (2011). Basophil recruitment and activation in inflammatory skin diseases. Allergy *66*, 1107–1113.

Jaworek, A.K., Szafraniec, K., Jaworek, M., Doniec, Z., Zalewski, A., Kurzawa, R., Wojas-Pelc, A., and Pokorski, M. (2020). Cat Allergy as a Source Intensification of Atopic Dermatitis in Adult Patients. Adv. Exp. Med. Biol. *1251*, 39–47.

Justiz Vaillant, A.A., and Jan, A. (2020). Atopy (StatPearls Publishing).

Kabashima, K., Furue, M., Hanifin, J.M., Pulka, G., Wollenberg, A., Galus, R., Etoh, T., Mihara, R., Nakano, M., and Ruzicka, T. (2018). Nemolizumab in patients with moderate-to-severe atopic dermatitis: Randomized, phase II, long-term extension study. J. Allergy Clin. Immunol. *142*, 1121–1130.e7.

Kim, B.S., Siracusa, M.C., Saenz, S.A., Noti, M., Monticelli, L.A., Sonnenberg, G.F., Hepworth, M.R., Van Voorhees, A.S., Comeau, M.R., and Artis, D. (2013). TSLP elicits IL-33-independent innate lymphoid cell responses to promote skin inflammation. Sci. Transl. Med. *5*, 170ra16.

Kim, B.S., Wang, K., Siracusa, M.C., Saenz, S.A., Brestoff, J.R., Monticelli, L.A., Noti, M., Tait Wojno, E.D., Fung, T.C., Kubo, M., and Artis, D. (2014a). Basophils promote innate lymphoid cell responses in inflamed skin. J. Immunol. *193*, 3717–3725.

Kim, Y.S., Chu, Y., Han, L., Li, M., Li, Z., LaVinka, P.C., Sun, S., Tang, Z., Park, K., Caterina, M.J., et al. (2014b). Central terminal sensitization of TRPV1 by descending serotonergic facilitation modulates chronic pain. Neuron *81*, 873–887.

Kim, M., Kim, Y.M., Lee, J.Y., Yang, H.K., Kim, H., Cho, J., Ahn, K., and Kim, J. (2017). Seasonal variation and monthly patterns of skin symptoms in Korean children with atopic eczema/dermatitis syndrome. Allergy Asthma Proc. *38*, 294–299.

Kim, B.S., Berger, T.G., and Yosipovitch, G. (2019). Chronic pruritus of unknown origin (CPUO): Uniform nomenclature and diagnosis as a pathway to standardized understanding and treatment. J. Am. Acad. Dermatol. *81*, 1223–1224.

Kim, B.S., Howell, M.D., Sun, K., Papp, K., Nasir, A., and Kuligowski, M.E.; INCB 18424-206 Study Investigators (2020a). Treatment of atopic dermatitis with ruxolitinib cream (JAK1/JAK2 inhibitor) or triamcinolone cream. J. Allergy Clin. Immunol. *145*, 572–582.

Kim, B.S., Sun, K., Papp, K., Venturanza, M., Nasir, A., and Kuligowski, M.E. (2020b). Effects of Ruxolitinib Cream on Pruritus and Quality of Life in Atopic Dermatitis: Results From a Phase 2, Randomized, Dose-Ranging, Vehicle- and Active-Controlled Study. J. Am. Acad. Dermatol. *82*, 1305–1313.

Kini, S.P., DeLong, L.K., Veledar, E., McKenzie-Brown, A.M., Schaufele, M., and Chen, S.C. (2011). The impact of pruritus on quality of life: the skin equivalent of pain. Arch. Dermatol. *147*, 1153–1156.

Krämer, U., Weidinger, S., Darsow, U., Möhrenschlager, M., Ring, J., and Behrendt, H. (2005). Seasonality in symptom severity influenced by temperature or grass pollen: results of a panel study in children with eczema. J. Invest. Dermatol. *124*, 514–523.

Langan, S.M., Thomas, K.S., and Williams, H.C. (2006). What is meant by a "flare" in atopic dermatitis? A systematic review and proposal. Arch. Dermatol. *142*, 1190–1196.

Larson, V.A., Tang, O., Ständer, S., Kang, S., and Kwatra, S.G. (2019). Association between itch and cancer in 16,925 patients with pruritus: Experience at a tertiary care center. J. Am. Acad. Dermatol. *80*, 931–937.

Letourneau, R., Pang, X., Sant, G.R., and Theoharides, T.C. (1996). Intragranular activation of bladder mast cells and their association with nerve processes in interstitial cystitis. Br. J. Urol. *77*, 41–54.

Lett-Brown, M.A., Aelvoet, M., Hooks, J.J., Georgiades, J.A., Thueson, D.O., and Grant, J.A. (1981). Enhancement of basophil chemotaxis in vitro by virus-induced interferon. J. Clin. Invest. *67*, 547–552.

Li, F., Yang, W., Jiang, H., Guo, C., Huang, A.J.W., Hu, H., and Liu, Q. (2019). TRPV1 activity and substance P release are required for corneal cold nociception. Nat. Commun. *10*, 5678.

Liu, Q., Tang, Z., Surdenikova, L., Kim, S., Patel, K.N., Kim, A., Ru, F., Guan, Y., Weng, H.J., Geng, Y., et al. (2009). Sensory neuron-specific GPCR Mrgprs are itch receptors mediating chloroquine-induced pruritus. Cell *139*, 1353–1365.

Liu, X.Y., Liu, Z.C., Sun, Y.G., Ross, M., Kim, S., Tsai, F.F., Li, Q.F., Jeffry, J., Kim, J.Y., Loh, H.H., and Chen, Z.F. (2011). Unidirectional cross-activation of GRPR by MOR1D uncouples itch and analgesia induced by opioids. Cell *147*, 447–458.

Liu, B., Tai, Y., Achanta, S., Kaelberer, M.M., Caceres, A.I., Shao, X., Fang, J., and Jordt, S.E. (2016). IL-33/ST2 signaling excites sensory neurons and mediates itch response in a mouse model of poison ivy contact allergy. Proc. Natl. Acad. Sci. USA *113*, E7572–E7579.

Luster, A.D., and Tager, A.M. (2004). T-cell trafficking in asthma: lipid mediators grease the way. Nat. Rev. Immunol. *4*, 711–724.

Mancini, J.A., Abramovitz, M., Cox, M.E., Wong, E., Charleson, S., Perrier, H., Wang, Z., Prasit, P., and Vickers, P.J. (1993). 5-lipoxygenase-activating protein is an arachidonate binding protein. FEBS Lett. *318*, 277–281.

Marshall, J.S. (2004). Mast-cell responses to pathogens. Nat. Rev. Immunol. *4*, 787–799.

Mashiko, S., Mehta, H., Bissonnette, R., and Sarfati, M. (2017). Increased frequencies of basophils, type 2 innate lymphoid cells and Th2 cells in skin of patients with atopic dermatitis but not psoriasis. J. Dermatol. Sci. *88*, 167–174.

McGowan, E.C., Bloomberg, G.R., Gergen, P.J., Visness, C.M., Jaffee, K.F., Sandel, M., O'Connor, G., Kattan, M., Gern, J., and Wood, R.A. (2015). Influence of early-life exposures on food sensitization and food allergy in an inner-city birth cohort. J. Allergy Clin. Immunol. *135*, 171–178.

Meixiong, J., Anderson, M., Limjunyawong, N., Sabbagh, M.F., Hu, E., Mack, M.R., Oetjen, L.K., Wang, F., Kim, B.S., and Dong, X. (2019). Activation of Mast-Cell-Expressed Mas-Related G-Protein-Coupled Receptors Drives Non-histaminergic Itch. Immunity *50*, 1163–1171.e5.

Min, B., Prout, M., Hu-Li, J., Zhu, J., Jankovic, D., Morgan, E.S., Urban, J.F., Jr., Dvorak, A.M., Finkelman, F.D., LeGros, G., and Paul, W.E. (2004). Basophils produce IL-4 and accumulate in tissues after infection with a Th2-inducing parasite. J. Exp. Med. *200*, 507–517.

Mishra, S.K., and Hoon, M.A. (2013). The cells and circuitry for itch responses in mice. Science *340*, 968–971.

Miyake, K., and Karasuyama, H. (2017). Emerging roles of basophils in allergic inflammation. Allergol. Int. *66*, 382–391.

Mukai, K., Matsuoka, K., Taya, C., Suzuki, H., Yokozeki, H., Nishioka, K., Hirokawa, K., Etori, M., Yamashita, M., Kubota, T., et al. (2005). Basophils play a critical role in the development of IgE-mediated chronic allergic inflammation independently of T cells and mast cells. Immunity *23*, 191–202.

Mukai, K., Chinthrajah, R.S., Nadeau, K.C., Tsai, M., Gaudenzio, N., and Galli, S.J. (2017). A new fluorescent-avidin-based method for quantifying basophil activation in whole blood. J. Allergy Clin. Immunol. *140*, 1202–1206.e3.

Noti, M., Wojno, E.D., Kim, B.S., Siracusa, M.C., Giacomin, P.R., Nair, M.G., Benitez, A.J., Ruymann, K.R., Muir, A.B., Hill, D.A., et al. (2013). Thymic stromal lymphopoietin-elicited basophil responses promote eosinophilic esophagitis. Nat. Med. *19*, 1005–1013.

Oetjen, L.K., Mack, M.R., Feng, J., Whelan, T.M., Niu, H., Guo, C.J., Chen, S., Trier, A.M., Xu, A.Z., Tripathi, S.V., et al. (2017). Sensory Neurons Co-opt Classical Immune Signaling Pathways to Mediate Chronic Itch. Cell *171*, 217–228.e13.

Ogawa, Y., Kono, M., Tsujikawa, M., Tsujiuchi, H., and Akiyama, M. (2016). IgE-independent pathophysiology of severe atopic dermatitis demonstrated in an IgE-deficient patient. J. Dermatol. Sci. *82*, 139–141.

Phan, N.Q., Blome, C., Fritz, F., Gerss, J., Reich, A., Ebata, T., Augustin, M., Szepietowski, J.C., and Ständer, S. (2012). Assessment of pruritus intensity: prospective study on validity and reliability of the visual analogue scale, numerical rating scale and verbal rating scale in 471 patients with chronic pruritus. Acta Derm. Venereol. *92*, 502–507.

Raap, U., Gehring, M., Kleiner, S., Rüdrich, U., Eiz-Vesper, B., Haas, H., Kapp, A., and Gibbs, B.F. (2017). Human basophils are a source of - and are differentially activated by - IL-31. Clin. Exp. Allergy *47*, 499–508.

Rajagopalan, M., Saraswat, A., Godse, K., Shankar, D.S., Kandhari, S., Shenoi, S.D., Tahiliani, S., and Zawar, V.V. (2017). Diagnosis and Management of Chronic Pruritus: An Expert Consensus Review. Indian J. Dermatol. *62*, 7–17.

Rappel, W.J., and Edelstein-Keshet, L. (2017). Mechanisms of Cell Polarization. Curr. Opin. Syst. Biol. *3*, 43–53.

Ruzicka, T., Hanifin, J.M., Furue, M., Pulka, G., Mlynarczyk, I., Wollenberg, A., Galus, R., Etoh, T., Mihara, R., Yoshida, H., et al.; XCIMA Study Group (2017). Anti-Interleukin-31 Receptor A Antibody for Atopic Dermatitis. N. Engl. J. Med. *376*, 826–835.

Sasaki, F., and Yokomizo, T. (2019). The leukotriene receptors as therapeutic targets of inflammatory diseases. Int. Immunol. *31*, 607–615.

Schauberger, E., Peinhaupt, M., Cazares, T., and Lindsley, A.W. (2016). Lipid Mediators of Allergic Disease: Pathways, Treatments, and Emerging Therapeutic Targets. Curr. Allergy Asthma Rep. *16*, 48.

Silverberg, J.I., Pinter, A., Pulka, G., Poulin, Y., Bouaziz, J.D., Wollenberg, A., Murrell, D.F., Alexis, A., Lindsey, L., Ahmad, F., et al. (2020). Phase 2B randomized study of nemolizumab in adults with moderate-to-severe atopic dermatitis and severe pruritus. J. Allergy Clin. Immunol. *145*, 173–182.

Simpson, E.L., Bieber, T., Guttman-Yassky, E., Beck, L.A., Blauvelt, A., Cork, M.J., Silverberg, J.I., Deleuran, M., Kataoka, Y., Lacour, J.P., et al.; SOLO 1 and SOLO 2 Investigators (2016). Two Phase 3 Trials of Dupilumab versus Placebo in Atopic Dermatitis. N. Engl. J. Med. *375*, 2335–2348.

Solinski, H.J., Kriegbaum, M.C., Tseng, P.Y., Earnest, T.W., Gu, X., Barik, A., Chesler, A.T., and Hoon, M.A. (2019). Nppb Neurons Are Sensors of Mast Cell-Induced Itch. Cell Rep. *26*, 3561–3573.e4.

Sommer, F., Hensen, P., Böckenholt, B., Metze, D., Luger, T.A., and Ständer, S. (2007). Underlying diseases and co-factors in patients with severe chronic pruritus: a 3-year retrospective study. Acta Derm. Venereol. *87*, 510–516.

Spergel, J.M., and Paller, A.S. (2003). Atopic dermatitis and the atopic march. J. Allergy Clin. Immunol. *112* (*Suppl 6*), S118–S127.

Spergel, J.M., Mizoguchi, E., Oettgen, H., Bhan, A.K., and Geha, R.S. (1999). Roles of TH1 and TH2 cytokines in a murine model of allergic dermatitis. J. Clin. Invest. *103*, 1103–1111.

Ständer, S., Blome, C., Anastasiadou, Z., Zeidler, C., Jung, K.A., Tsianakas, A., Neufang, G., and Augustin, M. (2017). Dynamic Pruritus Score: Evaluation of the Validity and Reliability of a New Instrument to Assess the Course of Pruritus. Acta Derm. Venereol. *97*, 230–234.

Ständer, S., Yosipovitch, G., Legat, F.J., Lacour, J.P., Paul, C., Narbutt, J., Bieber, T., Misery, L., Wollenberg, A., Reich, A., et al. (2020). Trial of Nemolizumab in Moderate-to-Severe Prurigo Nodularis. N. Engl. J. Med. *382*, 706–716.

Stead, R.H., Tomioka, M., Quinonez, G., Simon, G.T., Felten, S.Y., and Bienenstock, J. (1987). Intestinal mucosal mast cells in normal and nematode-infected rat intestines are in intimate contact with peptidergic nerves. Proc. Natl. Acad. Sci. USA *84*, 2975–2979.

Steinhoff, M., Buddenkotte, J., and Lerner, E.A. (2018). Role of mast cells and basophils in pruritus. Immunol. Rev. *282*, 248–264.

Sullivan, B.M., Liang, H.E., Bando, J.K., Wu, D., Cheng, L.E., McKerrow, J.K., Allen, C.D., and Locksley, R.M. (2011). Genetic analysis of basophil function in vivo. Nat. Immunol. *12*, 527–535.

Sun, Y.G., and Chen, Z.F. (2007). A gastrin-releasing peptide receptor mediates the itch sensation in the spinal cord. Nature *448*, 700–703.

Sun, S., and Dong, X. (2016). Trp channels and itch. Semin. Immunopathol. *38*, 293–307.

Suzukawa, M., Hirai, K., Iikura, M., Nagase, H., Komiya, A., Yoshimura-Uchiyama, C., Yamada, H., Ra, C., Ohta, K., Yamamoto, K., and Yamaguchi,

M. (2005). IgE- and FcepsilonRI-mediated migration of human basophils. Int. Immunol. *17*, 1249–1255.

Undem, B.J., Riccio, M.M., Weinreich, D., Ellis, J.L., and Myers, A.C. (1995). Neurophysiology of mast cell-nerve interactions in the airways. Int. Arch. Allergy Immunol. *107*, 199–201.

Usoskin, D., Furlan, A., Islam, S., Abdo, H., Lönnerberg, P., Lou, D., Hjerling-Leffler, J., Haeggström, J., Kharchenko, O., Kharchenko, P.V., et al. (2015). Unbiased classification of sensory neuron types by large-scale single-cell RNA sequencing. Nat. Neurosci. *18*, 145–153.

Veldhuis, N.A., Poole, D.P., Grace, M., McIntyre, P., and Bunnett, N.W. (2015). The G protein-coupled receptor-transient receptor potential channel axis: molecular insights for targeting disorders of sensation and inflammation. Pharmacol. Rev. *67*, 36–73.

Vocks, E., Busch, R., Fröhlich, C., Borelli, S., Mayer, H., and Ring, J. (2001). Influence of weather and climate on subjective symptom intensity in atopic eczema. Int. J. Biometeorol. *45*, 27–33.

Voehringer, D. (2013). Protective and pathological roles of mast cells and basophils. Nat. Rev. Immunol. *13*, 362–375.

Voehringer, D. (2017). Recent advances in understanding basophil functions *in vivo*. F1000Res. *6*, 1464.

Walsh, C.M., Hill, R.Z., Schwendinger-Schreck, J., Deguine, J., Brock, E.C., Kucirek, N., Rifi, Z., Wei, J., Gronert, K., Brem, R.B., et al. (2019). Neutrophils promote CXCR3-dependent itch in the development of atopic dermatitis. eLife *8*, e48448.

Wang, B., Zinselmeyer, B.H., Runnels, H.A., LaBranche, T.P., Morton, P.A., Kreisel, D., Mack, M., Nickerson-Nutter, C., Allen, P.M., and Miller, M.J. (2012). In vivo imaging implicates CCR2(+) monocytes as regulators of neutrophil recruitment during arthritis. Cell. Immunol. *278*, 103–112.

Wang, F., Yang, T.B., and Kim, B.S. (2020). The Return of the Mast Cell: New Roles in Neuroimmune Itch Biology. J. Invest. Dermatol. *140*, 945–951.

Wardlaw, A.J., Walsh, G.M., and Symon, F.A. (1994). Mechanisms of eosinophil and basophil migration. Allergy *49*, 797–807.

Wassmann-Otto, A., Heratizadeh, A., Wichmann, K., and Werfel, T. (2018). Birch pollen-related foods can cause late eczematous reactions in patients with atopic dermatitis. Allergy *73*, 2046–2054.

Wedi, B., Gehring, M., and Kapp, A. (2020). The pseudoallergen receptor MRGPRX2 on peripheral blood basophils and eosinophils: Expression and function. Allergy *75*, 2229–2242.

Weidinger, S., Beck, L.A., Bieber, T., Kabashima, K., and Irvine, A.D. (2018). Atopic dermatitis. Nat. Rev. Dis. Primers *4*, 1.

Weisshaar, E., Ziethen, B., and Gollnick, H. (1997). Can a serotonin type 3 (5-HT3) receptor antagonist reduce experimentally-induced itch? Inflamm. Res. *46*, 412–416.

Werfel, T., Heratizadeh, A., Niebuhr, M., Kapp, A., Roesner, L.M., Karch, A., Erpenbeck, V.J., Lösche, C., Jung, T., Krug, N., et al. (2015). Exacerbation of atopic dermatitis on grass pollen exposure in an environmental challenge chamber. J. Allergy Clin. Immunol. *136*, 96–103.e9.

Williams, H.C., Burney, P.G., Hay, R.J., Archer, C.B., Shipley, M.J., Hunter, J.J., Bingham, E.A., Finlay, A.Y., Pembroke, A.C., Graham-Brown, R.A., et al. (1994). The U.K. Working Party's Diagnostic Criteria for Atopic Dermatitis. I. Derivation of a minimum set of discriminators for atopic dermatitis. Br. J. Dermatol. *131*, 383–396.

Wilson, S.R., Thé, L., Batia, L.M., Beattie, K., Katibah, G.E., McClain, S.P., Pellegrino, M., Estandian, D.M., and Bautista, D.M. (2013). The epithelial cell-derived atopic dermatitis cytokine TSLP activates neurons to induce itch. Cell *155*, 285–295.

STAR★METHODS

KEY RESOURCES TABLE

REAGENT or RESOURCE	SOURCE	IDENTIFIER
Antibodies		
anti-mouse CD16/CD32	Bio X Cell	Cat#: BE0307; RRID: AB_1107647
anti-mouse CD49b	Invitrogen	Cat#: 17-5971-82; RRID: AB_469485
anti-mouse CD117 (c-kit)	Biolegend	Cat#: 135122; RRID: AB_2562042
anti-mouse CD5	eBioscience	Cat#: 45-0051-82; RRID: AB_914334
anti-mouse CD3e	eBioscience	Cat#: 45-0031-82; RRID: AB_1107000
anti-mouse CD11c	eBioscience	Cat#: 45-0114-82; RRID: AB_925727
anti-mouse CD19	eBioscience	Cat#: 45-0193-82; RRID: AB_1106999
anti-mouse NK1.1	eBioscience	Cat#: 45-5941-82; RRID: AB_914361
anti-mouse IgE	eBioscience	Cat#: 11-5992-81; RRID: AB_465342
anti-mouse FcεR1 alpha	eBioscience	Cat#: 11-5898-82; RRID: AB_465308
anti-mouse CD200R	Biolegend	Cat#: 123908; RRID: AB_2074080
anti-mouse CD45	Biolegend	Cat#: 103113; RRID: AB_312978
anti-mouse CD117 (c-kit)	eBioscience	Cat#: 25-1171-82; RRID: AB_469644
anti-mouse CD200R3	Biolegend	Cat#: 142211; RRID: AB_2814045
Biotin anti-mouse CD4	Biolegend	Cat#: 100508; RRID: AB_312711
Biotin anti-mouse CD8a	Biolegend	Cat#: 100704; RRID: AB_312743
Biotin anti-mouse CD11c	Biolegend	Cat#: 117304; RRID: AB_313773
Biotin anti-mouse/human CD45R/B220	Biolegend	Cat#: 103204; RRID: AB_312989
anti-human CD45	Biolegend	Cat#: 368514; RRID: AB_2566374
anti-human CD3	Biolegend	Cat#: 300318; RRID: AB_314054
anti-human CD4	Biolegend	Cat#: 317442; RRID: AB_2563242
anti-human CD123	Biolegend	Cat#: 306010; RRID: AB_493576
anti-human FcεRIα	Biolegend	Cat#: 334626; RRID: AB_2564291
anti-human CD203c (E-NPP3)	Biolegend	Cat#: 324620; RRID: AB_2563849
anti-human CD117 (c-kit)	Biolegend	Cat#: 313226; RRID: AB_2566213
anti-human CD34	Biolegend	Cat#: 343604; RRID: AB_1732005
anti-human CD56 (NCAM)	Biolegend	Cat#: 318303; RRID: AB_604091
anti-human CD14	Biolegend	Cat#: 325604; RRID: AB_830677
anti-human CD19	Biolegend	Cat#: 302206; RRID: AB_314236
Mouse anti-OVA IgE	Bio-Rad	Cat#: MCA2259; RRID:AB_2285753
Purified anti-mouse CD200R3	Biolegend	Cat#: 142204; RRID: AB_10945156
Purified Rat IgG2a, κ Isotype Ctrl	Biolegend	Cat#: 400533; RRID:AB_2861021
CysLT2 Receptor Antibody (B-7)	Santa Cruz Biotechnology	Cat#: sc-514181
m-IgGκ BP-FITC	Santa Cruz Biotechnology	Cat#: sc-516140
Anti-PGP9.5 antibody	Abcam	Cat#: ab10410; RRID:AB_297150
Cy3 AffiniPure Donkey Anti-Guinea Pig IgG (H+L)	Jackson ImmunoResearch	Cat#: 706-165-148 RRID: AB_2340460
Chemicals, peptides, and recombinant proteins		
Calcipotriol (MC903)	Tocris Bioscience	Cat#: 2700
Ovalbumin	Sigma-Aldrich	Cat#: A5503
Bovine Serum Albumin	Sigma-Aldrich	Cat#: A9418
Normal Goat Serum	Abcam	Cat#: ab7841
Avidin, Texas Red Conjugate	Invitrogen	Cat#: A820

(*Continued on next page*)

Continued

REAGENT or RESOURCE	SOURCE	IDENTIFIER
Qtracker 655 Vascular Labels	Invitrogen	Cat#: Q21021MP
Clozapine-N-oxide	Hello Bio	Cat#: HB 1807
Diphtheria Toxin	Sigma-Aldrich	Cat#: D0564
Olopatadine	Sigma-Aldrich	Cat#: O0391
JNJ7777120	Sigma-Aldrich	Cat#: J3770
FSLLRY-NH2	Sigma-Aldrich	Cat#: SML0714
Zileuton	Sigma-Aldrich	Cat#: Z4277
p-Chlorophenylalanine	Tocris Bioscience	Cat#: 0938
HAMI3379	Cayman	Cat#: 10580
Zafirlukast	Sigma-Aldrich	Cat#: Z4152
CP-105,696	Sigma-Aldrich	Cat#: PZ0363
Dispase II	GIBCO	Cat#: 17105041
Collagenase Type I	GIBCO	Cat#: 17100-017
Nerve Growth Factor	Sigma-Aldrich	Cat#: N6009
Glial-Derived Neurotrophic Factor	Sigma-Aldrich	Cat#: SRP3200
Fura-2 AM	Invitrogen	Cat#: F1201
Neurobasal-A	GIBCO	Cat#: 10888022
B-27 Supplement	GIBCO	Cat#: 17504001
Histamine	Sigma-Aldrich	Cat#: H7250
N-methyl Leukotriene C4	Cayman	Cat#: 13390
Allyl Isothiocyanate	Sigma-Aldrich	Cat#: W203408
Capsaicin	Sigma-Aldrich	Cat#: M2028
β-alanine	Sigma-Aldrich	Cat#: A9920
Chloroquine	Sigma-Aldrich	Cat#: C6628
Serotonin	Sigma-Aldrich	Cat#: H9523
Fetal Bovine Serum	Sigma-Aldrich	Cat#: 2442
Penicillin-Streptomycin	GIBCO	Cat#: 15140122
L-Glutamine	Corning	Cat#: MT25005CI
2-Mercaptoethanol	GIBCO	Cat#: 21985-023
Sodium Pyruvate	Corning	Cat#: 25-000-CI
MEM Nonessential Amino Acids	Corning	Cat#: 25-025-CI
Hu FcR Binding Inhibitor	eBioscience	Cat#: 14-9161-73
RVG-9R trifluoroacetate salt	BACHEM	Cat#: 4058134.0500
siGENOME Non-Targeting siRNA Control Pools	Horizon	Cat#: D-001206-14-20
siGENOME Mouse Cysltr2 siRNA	Horizon	Cat#: M-051452-01-0010
Glucose Solution	Fisher Scientific	Cat#: A2494001
UltraCruz Blocking Reagent	Santa Cruz Biotechnology	Cat#: sc-516214
Imject Alum	Thermo Scientific	Cat#: 77161
Zombie UV Fixable Viability Kit	Biolegend	Cat#: 423107
Critical commercial assays		
Mouse OVA-IgE ELISA kit	Biolegend	Cat#: 439807
Mouse Leukotriene B4 ELISA Kit	Biomatik	Cat#: EKC37285
Mouse Leukotriene C4 ELISA Kit	LS Bio	Cat#: LS-F28464-1
Mouse Streptavidin RapidSpheres Isolation Kit	STEMCELL	Cat#: 19860
Experimental models: organisms/strains		
C57BL/6J	Jackson Laboratory	Stock No. 000664
Sash$^{-/-}$	Jackson Laboratory	Stock No. 030764

(*Continued on next page*)

Continued

REAGENT or RESOURCE	SOURCE	IDENTIFIER
Mcpt8-Cre	Jackson Laboratory	Stock No. 017578
R26-LSL-Gq-DREADD	Jackson Laboratory	Stock No. 026220
Ai9	Jackson Laboratory	Stock No. 007909
Alox5$^{-/-}$	Jackson Laboratory	Stock No. 004155
$Na_V1.8$-Cre	Rohini Kuner (Heidelberg University)	N/A
Bas-TRECK	Masato Kubo (RIKEN, Yokohama Institute, Japan)	N/A
Ige$^{-/-}$	Masato Kubo (RIKEN, Yokohama Institute, Japan)	N/A
Pirt$^{GCamp3/+}$	Xinzhong Dong (Johns Hopkins University School of Medicine)	N/A
Trpv1$^{-/-}$	Jackson Laboratory	Stock No. 003770
Trpa1$^{-/-}$	Jackson Laboratory	Stock No. 006401
Compound *Trpv1*$^{-/-}$ *Trpa1*$^{-/-}$	Hongzhen Hu (Washington University)	N/A
Software and algorithms		
FlowJo 10	Tree Star	https://www.flowjo.com/
Prism 8	GraphPad Software	https://www.graphpad.com:443/scientific-software/prism/
NIS-Elements	Nikon Instruments	https://www.microscope.healthcare.nikon.com/products/software
Imaris 9	Bitplane	https://imaris.oxinst.com/
Others		
NanoZoomer 2.0-HT System	Hamamatsu	N/A
LSRFortessa X-20	BD Biosciences	N/A
Nikon Ti-S Microscope	Nikon Instruments	N/A
CoolSNAP HQ_2 CCD camera	Photometrics	N/A
Nikon AI Confocal Microscope System	Nikon Instruments	N/A
Chameleon Vision II Ti:Sapphire Lasers	Coherent	N/A

RESOURCE AVAILABILITY

Lead contact

Further information and requests for resources and reagents should be directed to and will be fulfilled by the Lead Contact, Brian S. Kim (briankim@wustl.edu).

Materials availability

This study did not generate new unique reagents.

Data and code availability

This study did not generate any unique datasets or code. All other data supporting the findings of this study are available in the manuscript or the supplementary materials and available upon request to the lead contact author.

EXPERIMENTAL MODEL AND SUBJECT DETAILS

Human subjects

For analysis of itch pattern and allergen-specific IgE related to atopic dermatitis (AD), numerical rating scale (NRS) itch scores and serum allergen-specific IgE repertoire were respectively reviewed on N = 159 subjects from the placebo group of the SOLO1 and SOLO2 phase 3 clinical trials (Simpson et al., 2016). Patient serum allergen-specific IgE repertoires were measured using the ImmunoCAP system (Phadia AB, Uppsala, Sweden) for a panel of 12 allergens/antigens including *Dermatophagoides pteronyssinus*, *Dermatophagoides farinae*, *Canadida albicans*, *Pityrosporum*, cat dander, mountain juniper, white oak, olive tree, Staphylococcal

enterotoxin A, Staphylococcal enterotoxin B, Japanese cedar, and wall pellitory. Positive levels for each allergen were defined as an allergen-specific IgE concentration $\geq$ 0.35 kU/L (McGowan et al., 2015).

In order to examine human basophil phenotypes, 12 adult patients with AD, who visited the Dermatology Clinic at the Perelman School of Medicine at the University of Pennsylvania from October 2018 to June 2019, and 12 age- and sex-matched healthy controls were recruited. Patients were diagnosed with AD according to the UK Working Party's Diagnostic Criteria (Williams et al., 1994). The disease severity was assessed according to Patient Oriented Eczema Measure (POEM) (Charman et al., 2013). After informed consent was obtained, peripheral blood was collected and peripheral blood mononuclear cells (PBMCs) were isolated by Ficoll density gradient purification and frozen at -80°C until assayed. These studies were conducted in accordance with the provisions of the Declaration of Helsinki and International Conference on Harmonisation Good Clinical Practice guidelines. All the patients provided written informed consent before participation in the studies. The local institutional review board or ethics committee at each study center oversaw study conduct and documentation.

Research animals

Wild-type (WT) C56Bl/6J, C57BL/6-*Kit*$^{W\text{-}sh/W\text{-}sh}$ (also known as *Sash*$^{-/-}$), *Mcpt8*-Cre, R26-LSL-Gq-DREADD, Ai9, and *Alox5*$^{-/-}$ mice were purchased from Jackson Laboratories. Bas-TRECK and *Ige*$^{-/-}$ mice were donated by Dr. Masato Kubo (RIKEN, Yokohama Institute, Japan). Compound *Trpv1*$^{-/-}$ *Trpa1*$^{-/-}$ double-deficient mice were donated by Dr. Hongzhen Hu. Na_V1.8-Cre mice were provided by Dr. Rohini Kuner (Heidelberg University). *Pirt*$^{GCamp3/+}$ mice were donated by Dr. Xinzhong Dong. *Mcpt8*-Cre:R26-LSL-Gq-DREADD mice were obtained by crossing *Mcpt8*-Cre animals with R26-LSL-Gq-DREADD animals. Na_V1.8-TdTomato mice were generated by crossing Na_V1.8-Cre mice with Ai9 mice. All experiments were conducted with the approval of the Washington University Institutional Animal Care and Use Committee. Animals were housed on a standard 12:12 hour light-dark cycle with free access to food and water. For dorsal root ganglia (DRG) neuron isolation, 4–6-week-old mice were used. For all other experiments, 8–12-week-old mice were used. Experiments were performed on independent cohorts of male and female mice and no differences between sexes were observed.

METHOD DETAILS

Mouse model

The right cheeks of mice were shaved 2 days prior to any treatments (day -2). To induce AD-associated acute itch flares, bilateral ear skin were topically treated with 0.5 nmol of MC903 (calcipotriol, Tocris Bioscience) in 15 μL of 100% ethanol and then with 20 μL of 5 mg/mL ovalbumin (OVA, Sigma-Aldrich) in phosphate-buffered saline (PBS) daily for 10 days (day 0 to day 9) to sensitize mice. Unsensitized control mice were treated with 15 μL of 100% ethanol (vehicle control) followed by 20 μL of 5 mg/mL OVA in PBS. On day 10, mice were given an intradermal (i.d.) injection of 20 μL of 2.5 mg/mL OVA in 0.9% saline in their right cheek in order to provoke acute itch responses. To test the specificity of the allergen response, sensitized (MC903 + OVA) mice were i.d. challenged with 20 μL of an irrelevant allergen, bovine serum albumin (BSA, 3.7 mg/mL in 0.9% saline; Sigma-Aldrich). As an alternative to this model, we passively sensitized mice with OVA in the setting of AD-like disease. AD-like disease was induced by topical MC903 (0.5 nmol in 15 μL of 100% ethanol) administration on bilateral ear skin of mice daily from day 0 to day 9. On day 8 and day 9, mice received an intravenous (i.v.) injection of 100 μL of 20 μg/mL anti-OVA IgE antibody (Bio-Rad) in PBS to induce passive sensitization. Control unsensitized mice received i.v injections with 100 μL PBS alone. On day 10, an acute itch flare was evoked by i.d. injection of 20 μL of 2.5 mg/mL OVA in 0.9% saline into the right cheek. To assess allergen-mediated acute itch in the steady state, mice were passively sensitized to OVA via i.v. injection of 100 μL of 20 μg/mL anti-OVA IgE antibody in PBS on day 0 and day 1. Control unsensitized mice received i.v. injections of 100 μL PBS alone. On day 2, mice were challenged i.d. with 20 μL of 2.5 mg/mL OVA in 0.9% saline in their right cheek to provoke acute itch. The systemic sensitization model was induced as previously described (Huang et al., 2016). In brief, OVA (0.2 mg/mL in PBS; Sigma-Aldrich) was prepared fresh each time and was emulsified with an equal volume of Imject Alum (alum; Thermo Scientific). Mice received an intraperitoneal (i.p.) injection of 200 μl of OVA + alum mixture or control PBS + alum mixture on day 0 and day 9. On day 13, mice were challenged i.d. with 20 μL of 2.5 mg/mL OVA in 0.9% saline in their right cheek. To test acute itch flares in the setting of systemic sensitization along with AD-like disease, we sensitized mice with i.p. injection of 200 μL of OVA + alum mixture (prepared as above) on day 0 and day 9. Concurrently, bilateral ear skin were treated topically with MC903 (0.5 nmol in 15 μL of 100% ethanol) from day 3 to day 12. To provoke acute itch flares, mice were challenged with i.d. injection of 20 μL of 2.5 mg/mL OVA in 0.9% saline in the right cheek on day 13. For all models, scratching behavior was recorded for 60 minutes before i.d. allergen (OVA or BSA) challenge and for 70 minutes after challenge.

Skin inflammation assessment and histopathology

To assess mouse ear skin inflammation induced by MC903 + OVA, ear thickness was measured daily with dial calipers as previously described (Kim et al., 2013, 2014a). Prior to i.d. OVA challenge on experimental day 10 of the AD-associated acute itch flare model, mice were euthanized and tissues were harvested for analysis. The ear skin were fixed in 4% paraformaldehyde (PFA; Thermo Scientific) and embedded in paraffin before sectioning and staining with Hematoxylin & Eosin (H&E). Slides were imaged using the NanoZoomer 2.0-HT System (Hamamatsu).

Pharmacologic treatments administration in mouse models

In our passive sensitization model, mice were treated with an i.p. injection of 100 μL the H1R antagonist olopatadine (3 mg/kg in PBS; Sigma-Aldrich) and subcutaneous (s.c.) injection (nape) with 100 μL of the H4R antagonist JNJ7777120 (20 mg/kg in PBS; Sigma-Aldrich) 30 minutes prior to i.d. OVA challenge.

In the AD-associated acute itch flare model, mice were treated 30 minutes prior to i.d. OVA challenge (day 10) with i.p. injection of 100 μL of the H1R antagonist olopatadine (3 mg/kg in of PBS; Sigma-Aldrich) and s.c. injection (nape) of 100 μL of the H4R antagonist JNJ7777120 (20 mg/kg in of PBS; Sigma-Aldrich). Protease-activated receptor 2 (PAR2) was blocked by the administration of 100 μL of FSLLRY-NH2 (7.5 mg/kg in 0.9% saline; Sigma-Aldrich) i.p. 30 minutes prior to i.d. OVA challenge (day 10). To inhibit serotonin synthesis, 200 μL of *p*-Chlorophenylalanine (pCPA, 150 mg/kg in 0.9% saline; Tocris Bioscience) was i.p. injected on day 7, day 8, and day 9 of the 10-day sensitization process. Mice were gavaged with 100 μL of the leukotriene (LT) pathway inhibitor zileuton (50 mg/kg in 0.5% cellulose; Sigma-Aldrich) 60 minutes prior to assessment of chronic spontaneous itch (day 10) or 60 minutes prior to i.d. OVA challenge when assessing acute itch flare behavior (day 10). The LTB4 receptor antagonist CP-105,696 (100 μL of 3 mg/kg CP-105,696 in 0.5% cellulose; Sigma-Aldrich) was administered by oral gavage 60 minutes prior to i.d. OVA challenge. Oral gavage of 100 μL of the CysLTR1 antagonist zafirlukast (10 mg/kg in PBS; Sigma-Aldrich) was given twice on day 9, and once on day 10, 60 minutes prior to i.d. OVA challenge. Mice were given two 100 μL i.p. injections of the CysLTR2 antagonist HAMI3379 (0.4 mg/kg in of PBS; Cayman) on day 9, and once on day 10, 60 minutes prior to assessment of chronic spontaneous itch (day 10) or 60 minutes prior to i.d. OVA challenge for the assessment of acute itch flare behavior (day 10).

Behavioral tests

All applicable behavioral tests were performed and analyzed with the experimenter blinded to genotype with the exception of the *Sash*$^{-/-}$ strain given the genotypic differences in coat color. Itch behavior experiments were performed between 8 a.m. and 12 p.m CST. Two days prior to recording, animals were habituated in the test chamber for 90 minutes and underwent a series of three mock i.d. injections where a capped needle was pressed against the shaved cheek of the experimental mouse. On the day of behavioral test, animals were allowed to acclimatize to the test chamber for 10 minutes prior to video recording. Video recordings were manually scored to assess the number of scratching bouts during a 30-minute period. A bout of scratching was defined as an instance of hind paw directed continuous scratching of the back, cheeks, or ears that ended when the mouse placed their hind paw in their mouth or to the chamber floor. To test the pruritogenic capability of *N*-methyl (N-met) LTC4, histamine and basophil-derived factors in supernatant, 20 μL of solution was i.d. injected into the shaved right cheeks of mice before immediate assessment of itch behavior. Only scratching bouts directed toward the site of injection were scored. For N-met LTC4 (Cayman) and histamine (Sigma-Aldrich), a range of doses were tested, 0–10,000 μg and 0–1.5 μg respectively. For basophil-derived factors, we collected supernatants from OVA-stimulated basophils. Briefly, 6×10^4– 8×10^4 basophils, sorted from mouse blood and cultured overnight, were incubated with 2.5 mg/ml OVA in 0.9% saline (200 μL) at 37°C and 5% CO_2 for 60 minutes. Collected supernatants was delivered i.d. undiluted (20 μL).

ELISA

To measure mouse serum OVA-specific IgE levels, 0.5–1 mL of blood was collected into 1.5 mL microcentrifuge tubes and allowed to clot for 60 minutes at room temperature. Tubes were then centrifuged for 10 minutes at 1,000 g at 4°C. Sera were collected and stored at −80°C until OVA-specific IgE was quantified using the mouse OVA-IgE ELISA kit (Biolegend) according to manufacturer's instructions.

To measure mouse serum LTB4 and LTC4 levels, 0.5–1 mL of blood was collected into 1.5 mL microcentrifuge tubes 30 minutes after allergen challenge and allowed to clot for 60 minutes at room temperature. Tubes were then centrifuged for 15 minutes at 1,000 g at 4°C. Serum was collected and stored at −80°C until LTB4 and LTC4 were respectively quantified using the mouse LTB4 ELISA kit (Biomatik) and mouse LTC4 ELISA kit (LS Bio) according to manufacturer's instructions.

To test supernatant levels of LTC4 derived from basophils, sort-purified basophils (6×10^4– 8×10^4 cells) were stimulated with 0.25 mg/mL OVA in 200 μL of saline at 37°C and 5% CO_2 in a 96 plate well for 60 minutes. After centrifuge for 20 minutes at 1,000 g at 4°C, supernatants were collected and stored at −80°C until LTC4 was quantified using the mouse LTC4 ELISA kit (LS Bio) according to manufacturer's instructions.

Flow cytometry

For human studies, thawed PBMCs were stained with Zombie UV viability dye (1:500; Biolegend) at room temperature for 20 minutes, washed and then stained with primary antibodies on ice for 30 minutes before being acquired on a BD Fortessa X-20 (BD Biosciences). Human Basophils were defined as live CD123$^+$ FcεRIα$^+$ cells that lacked expression of c-Kit and lineage (Lin) markers CD3, CD4, CD19, CD14, CD34, and CD56. Marker CD203c was included in the primary antibodies to reveal the activation state of human basophils.

For animal studies, 50–100 μL of blood was collected into EDTA coated tubes, followed by RBC lysis using RBC lysis buffer (Sigma-Aldrich) at room temperature for 5 minutes twice and washed by PBS once. All cells were stained with Zombie UV viability dye (1:500; Biolegend) for viability at room temperature for 20 minutes, followed by primary antibodies on ice for 30 minutes prior to data acquisition on a BD Fortessa X-20 (BD Biosciences). Basophils were defined as live CD49b$^+$ FcεRIα/IgE$^+$ cells that were negative for

expression of c-Kit and Lin markers CD3e, CD5, CD11c, CD19, and NK1.1. The mouse basophil canonical activation marker CD200R was also stained. All flow cytometry data were analyzed with Flowjo v10 software (Tree Star).

Immunofluorescence staining

Immunofluorescence imaging was performed as previously described (Huang et al., 2018). For ex *vivo* immunofluorescence staining of basophil degranulation in our AD-associated acute itch flare model, skin (OVA challenge site) from the right cheeks of *Sash*$^{-/-}$ mice were harvested 30 minutes following i.d. OVA challenge. Then, samples were fixed in 4% PFA (Thermo Scientific) for 4–6 hours at 4°C and incubated in 30% sucrose overnight. Tissues were embedded in optimal cutting temperature (OCT) medium (Sakura) and sectioned at 12 μm on a cryotome (Leica). Sections were dried and stained with 200 μL avidin-Texas Red (5 μg/mL; Invitrogen) in room temperature for 30 minutes before imaging on a Nikon Al Confocal Laser Microscope with NIS-Elements imaging software (Nikon Instruments).

To detect basophil degranulation *ex vivo*, 0.5–1 mL of blood from naive *Mcpt8*-Cre:R26-LSL-Gq-DREADD and littermate control *Mcpt8*-Cre-YFP mice was collected into EDTA-coated tubes. Samples were then treated with RBC lysis buffer (Sigma-Aldrich) at room temperature for 5 minutes twice and washed by PBS once. Following negative selection for CD4, CD8a, CD11c, and B220 using a Mouse Streptavidin RapidSpheres Isolation Kit (STEMCELL), purified leukocytes from each mouse were incubated with 200 μL clozapine-N-oxide (CNO, 400 μM in PBS; Hello Bio) and 200 μL avidin-Texas Red (5 μg/mL; Invitrogen) simultaneously for 30 minutes at room temperature before imaging on a Nikon Al Confocal Laser Microscope with NIS-Elements imaging software (Nikon Instruments).

To examine the knockdown effect of *in vivo* siRNA treatment, WT mice that received intracisternal injection of siRNA were euthanized on day 10 of the AD-associated acute itch flare model. Then mice trigeminal ganglia were dissected and fixed in 4% PFA (Thermo Scientific) for 4–6 hours at 4°C followed by incubation in 30% sucrose overnight. Tissues were embedded in OCT medium (Sakura) and sectioned at 12 μm on a cryotome (Leica). For further staining, sectioned tissues were blocked with 10% goat serum (Abcam) in UltraCruz blocking reagent (Santa Cruz Biotechnology) for 30 minutes and incubated with primary antibodies at 4 °C overnight. After rinsing, sections were incubated with secondary antibodies for 1 hour at room temperature. Images were taken and analyzed using a Nikon Al Confocal Laser Microscope with NIS-Elements imaging software (Nikon Instruments). Primary antibodies used: anti-CysLTR2 receptor monoclonal antibody (B-7; Santa Cruz Biotechnology; 1:100) and guinea pig anti-PGP9.5 polyclonal antibody (Abcam; 1:500). Secondary antibodies used: m-IgGκ BP-FITC (Santa Cruz Biotechnology; 1:100) and Cy3 AffiniPure donkey anti-guinea pig IgG (H+L) (Jackson ImmunoResearch; 1:500).

Basophil *in vivo* chemogenetic activation

To chemogenetically activate basophils *in vivo*, *Mcpt8*-Cre:R26-LSL-Gq-DREADD mice received a single i.p. injection of 50 μL of 1 mg/kg CNO (Hello Bio) in PBS. Mice were video recorded for 60 minutes after CNO injection and the itch behavior was quantified by manually counting the number of scratching bouts from 10 minutes to 40 minutes after CNO injection.

Basophil *in vivo* depletion

Basophil depletion was performed as previously described (Noti et al., 2013). Briefly, for pharmacologic depletion of basophils, WT mice received i.v. injections of 100 μL of purified anti-mouse CD200R3 antibody (1.0 mg/mL; Biolegend) or Rat IgG2a, κ isotype control (Biolegend) on day 7 and day 9 of the AD-associated acute itch flare model. For basophil genetic depletion, Bas-TRECK and littermate control mice were given an i.p. injection of 500 ng diphtheria toxin (DT; Sigma-Aldrich) diluted in 100 μL PBS daily on two consecutive days prior to the last day of the disease model. Specifically, in the AD-associated acute itch flare model (MC903 + OVA), mice were treated with DT i.p. on experimental day 8 and day 9. In the mouse model sensitized with i.p. OVA + alum, DT was i.p. injected on day 11 and day 12. The effect of depletion was confirmed by assessing blood basophil levels using flow cytometry prior to i.d. OVA challenge on the last day of each model.

Basophil sorting and cultures

Basophil sorting and cultures were performed as previously described (Hussain et al., 2018). Briefly, 0.5–1 mL of mouse blood was collected into EDTA coated tubes. Red blood cells were lysed using RBC lysis buffer (Sigma-Aldrich). All live, CD45^{+} Lin^{-} CD49b^{+} FcεRIα/IgE^{+} basophils from donor mice were sort-purified using an Aria II (BD Biosciences). Isolated basophils ($6 \times 10^4 - 8 \times 10^4$ cells /mL) were then cultured in Mast Cell Medium (RPMI 1640, 15% fetal bovine serum [FBS; Sigma-Aldrich], 100 U/mL penicillin [GIBCO], 100 μg/mL streptomycin [GIBCO], 2.9 mg/mL glutamine [Corning], 50 mM 2-mercaptoethanol [GIBCO], 1 mM sodium pyruvate [Corning], 1 × nonessential amino acids [Corning], 10 mM HEPES) overnight at 37°C and 5% CO_2 before further stimulation.

DRG neuronal cultures

Mouse DRG neurons were extracted, dissociated, and cultured as previously described (Kim et al., 2014b; Oetjen et al., 2017). Briefly, 4–6 week-old mice were euthanized by CO_2 inhalation. The DRGs were dissected and enzymatically dissociated with 1 mL Ca^{2+}/Mg^{2+}-free HBSS containing collagenase type I (342 U/mL; GIBCO) and dispase II (3.8 U/mL; GIBCO) for 30 minutes at 37°C. After digestion, neurons were gently triturated, pelleted, and then resuspended in Neurobasal-A culture medium (GIBCO) containing 2% B-27 supplement (GIBCO), 100 U/mL penicillin plus 100 mg/mL streptomycin (Sigma-Aldrich), 100 ng/mL nerve growth

factor (NGF, Sigma-Aldrich), 20 ng/mL glial cell-derived neurotrophic factor (GDNF; Sigma-Aldrich), and 10% FBS (Sigma-Aldrich). Neurons were then plated on 8 mm glass coverslips pre-coated with poly-D-lysine (PDL, 20 μg/mL) and laminin (20 μg/mL). Cells were cultured overnight at 37°C and 5% CO_2 before use in calcium imaging studies.

Calcium imaging of mouse DRG neurons

All reagents were applied to DRG neurons by perfusion except for basophil-derived factors, which were manually loaded by gently pipetting the culture supernatants into the recording chamber. Only sensory neurons that were responsive to a final challenge of KCl (50 mM) were used in downstream analyses. For cultured DRG neurons isolated from calcium reporter *Pirt*$^{GCaMP3/+}$ mice, fluorescence was recorded at 488 nm excitation wavelength using an inverted Nikon Ti-S microscope (Nikon Instruments) with CoolSNAP HQ_2 CCD camera (Photometrics) and NIS-elements software (Nikon Instruments). Cells were considered responsive to a particular stimulus if they exhibited at least a 15% increase in fluorescent intensity to baseline. For non-reporter mice (WT, *Trpv1*$^{-/-}$, *Trpa1*$^{-/-}$, and compound *Trpv1*$^{-/-}$ *Trpa1*$^{-/-}$ mice), cultured DRG neurons were first loaded with the calcium indicator dye Fura-2 AM (4 μM; Invitrogen) in DRG culture medium for 30 minutes at 37°C. Before use, cells were washed and incubated in calcium imaging buffer for at least 15 minutes at room temperature as previously described (Oetjen et al., 2017). Images were acquired with alternating 340 nm and 380 nm excitation wavelengths (F340, F380) using an inverted Nikon Ti-S microscope (Nikon Instruments) with CoolSNAP HQ_2 CCD camera (Photometrics) and NIS-elements software (Nikon Instruments). Cells were considered responsive if they demonstrated a change in fluorescence ratio (340/380) > 15% to baseline.

Basophil-derived factors were collected from OVA-stimulated cultures. Briefly, sort-purified and cultured basophils (6,000–8,000) were centrifuged for 5 minutes at 400 g at 4°C. Then, supernatants were carefully removed and the remaining basophils were stimulated with 0.25 mg/mL OVA in 200 μL of calcium imaging buffer at 37°C and 5% CO_2 for one hour. After centrifugation for 20 minutes at 1000 g at 4°C, supernatants were collected and applied to cultured DRG neurons (100 μL per culture slide) to test for neuronal activation as indicated by an intracellular calcium influx response. OVA solution (0.25 mg/mL in calcium imaging buffer) or N-met LTC4 (100 nM; Cayman) was applied by perfusion onto cultured DRG neurons to test for calcium responses. For additional characterization, responsiveness to the following reagents was also assessed: the TRPV1 agonist capsaicin (500 nM; Sigma-Aldrich); the TRPA1 agonist allyl isothiocyanate (AITC; 100 μM; Sigma-Aldrich); serotonin (5-HT) (200 μM; Sigma-Aldrich); β-alanine (1 mM; Sigma-Aldrich); and chloroquine (2 mM; Sigma-Aldrich).

Bone marrow transplant

Na_V1.8-TdTomato recipients were sublethally X-ray irradiated (950 cGy) using X-RAD 320 (Precision X-Ray). 10×10^6 bone marrow cells from *Mcpt8*-Cre-YFP mice were i.v. injected into the recipient mice within 24 hours after radiation. Sulfatrim (sulfamethoxazole/trimethoprim) was added to the drinking water of the irradiated animals (5mL/200mL) from one day prior to radiation until 1 week post-radiation and reconstitution. Irradiated mice were used for experimentation 8 weeks following bone marrow transplantation, allowing for full immune reconstitution. Chimerism was tested 4 weeks after reconstitution by measuring the presence of YFP^+ cells in the peripheral blood by flow cytometry.

Two-photon microscopy

In vivo two-photon imaging of cell trafficking was performed as previously described (Wang et al., 2012). Briefly, the right cheeks of mice were shaved the day prior to imaging. On day 10 of the AD-associated acute itch model, mice were anesthetized with isoflurane, placed on a warming pad and their right cheeks were secured to the imaging chamber using VetBond (cat #1469SB, 3 M). Time-lapse imaging was performed pre- and post-challenge with i.d. OVA by using a custom-built dual-laser video-rate two-photon microscope. To visualize blood vessels, 20 μL of non-targeted Qtracker 655 vascular labels (Invitrogen) were diluted in 100 μL of PBS and i.v. injected 15–30 minutes before imaging. Qtracker 655-labeled blood vessels and YFP-labeled basophils were excited by a Chameleon Vision II Ti:Sapphire laser (Coherent) tuned to 920 nm in *Mcpt8*-Cre-YFP mice. Fluorescence emission was detected as red (> 560 nm), green (495–560 nm), and blue (< 495 nm). To assess potential basophil-neuron interactions, YFP-labeled basophils and TdTomato-labeled nerves in bone marrow chimeric mice (*Mcpt8*-Cre × Na_V1.8-TdTomato) were excited by a Chameleon Vision II Ti:Sapphire laser (Coherent) tuned to 950 nm. Fluorescence emission was detected as red (> 540 nm), green (495–540 nm) and blue (< 495 nm). Each plane represents an image of 300 μm by 300 μm at 0.585 μm/pixel. Z stacks were acquired by taking 31 sequential steps at 2 μm spacing. Image reconstruction and multidimensional rendering were performed with Imaris (Bitplane). Cell track datasets were generated in Imaris using automated spot tracking and analyzed in MotilityLab (2Ptrack.net). In cases where motion artifacts induced z-plane tracking errors, cells were manually tracked using an orthogonal perspective in Imaris. To identify interactions between basophils and nerves, we inferred cell-cell contacts first by looking for evidence that the cells made apparent contacts with nerves in 3D rendered images. We then digitally zoomed into apparent contact regions and rotated them in 3D to confirm that green pixels (basophils) and red pixels (nerves) were in direct apposition. This was performed frame by frame in the videos to measure basophil-nerve interaction durations. The caveat to this approach is that we can only infer cell-cell interactions due to the limits of our image resolution, which is 0.585 μm in X and Y, and 2 μm in the Z-dimension. The interaction duration was then normalized to cell number by dividing the sum of apparent contact durations by the number of cells in each image.

Preparation and intracisternal injection of siRNA

We performed CysLTR2 siRNA knockdown *in vivo* by delivering siRNA using intracisternal (i.c.) injection as previously described (Li et al., 2019; Liu et al., 2011). The napes of the mice were shaved 2 days prior to the i.c. treatment. RVG-9R trifluoroacetate salt (BECHEM) was dissolved with 10% glucose (Fisher Scientific) to reach the concentration of 1.45 μg/μL. Meanwhile, siGENOME non-targeting siRNA control pools (Horizon) or siGENOME mouse CysLTR2 siRNA (Horizon) was dissolved with nuclease free water (Thermo Scientific) to reach the final concentration of 1 μg/μL. Before injection, 5 μL of RVG-9R (1.45 μg/μL in 10% glucose) was mixed with 5 μL of siRNA (1 μg/μL in nuclease free water) and incubated at room temperature for 15 minutes. To deliver the RVG-9R + siRNA mixture, adult WT mice were anesthetized with 2% isoflurane and then the mixture of RVG-9R and siRNA (10 μL) was injected slowly into the cisterna magna daily from day 7 to day 9 of the AD-associated acute itch flare model. On experimental day 10, trigeminal ganglia were dissected and stained for CysLTR2 to validate the knockdown effect.

QUANTIFICATION AND STATISTICAL ANALYSIS

Normally distributed group data were expressed as mean ± standard deviation (SD) and statistical significance was determined using the two-tailed Student's t test. If data were not normally distributed, median (interquartile range) was used and statistical significance was determined using the Wilcoxon–Mann–Whitney nonparametric test. For tests with multiple comparisons, the Two-way ANOVA test was used. Differences of incidence rate between two groups were compared by Chi-square test or Fisher's exact test when total N assessed in the contingency tables was less than 40 or when the expected frequency of one or more cells was less than 5. Data from independent experiments were pooled when possible or represent at least two independent replicates. Sample sizes were chosen based on pilot experiments to accurately detect statistical significance as well as considering technical feasibility, resource availability, and ethical animal and sample use. No samples or animals subjected to successful procedures and/or treatments were excluded from analysis. Statistical details can be found in figure legends. All statistical tests were conducted with GraphPad Prism 8. Significance is labeled as: ****$p < 0.0001$, ***$p < 0.001$, **$p < 0.01$, *$p < 0.05$, N.S., Not Significant.

Supplemental Figures

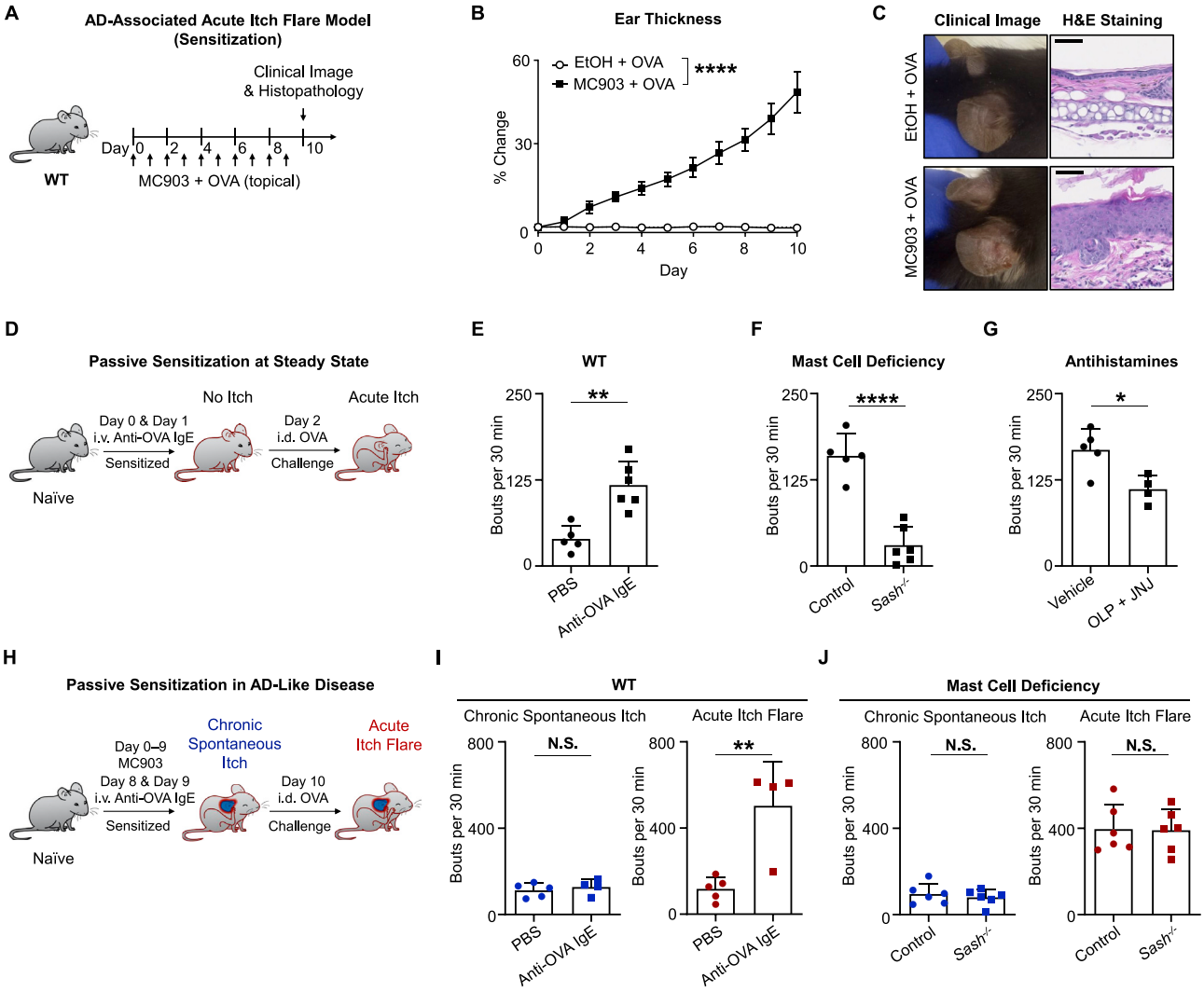

Figure S1. Allergen-provoked itch is dependent on mast cells and histamine in the steady state and becomes mast cell-independent in AD-like disease, related to Figure 1

(A) Schematic of allergen sensitization in the AD-associated acute itch flare model. Wild-type (WT) mice received daily topical treatment with calcipotriol (MC903) + ovalbumin (OVA) to bilateral ears from day 0 to day 9.

(B) Ear thickness (percent change from baseline) of vehicle ethanol (EtOH) control + OVA-treated and MC903 + OVA-treated WT mice from day 0 to day 10. n = 12–13 mice per group. ****$p < 0.0001$ by two-way ANOVA test.

(C) Representative clinical images (left) and H&E histopathology images (right) of lesional ear skin from EtOH control + OVA-treated and MC903 + OVA-treated WT mice on day 10 of the AD-like disease model. Scale bar = 50 μm.

(D) Schematic of naive mice that received intravenous (i.v.) injection of anti-OVA IgE antibody (passive sensitization) on day 0 and day 1 followed by intradermal (i.d.) OVA challenge into cheek and assessment of scratching behavior on day 2.

(E) Number of scratching bouts following i.d. OVA challenge in WT mice that were pretreated with i.v. phosphate-buffered saline (PBS) control or i.v. anti-OVA IgE antibody. n = 5–6 mice per group. **$p < 0.01$ by unpaired Student's t test.

(F) Number of scratching bouts following i.d. OVA challenge in sensitized (i.v. anti-OVA IgE antibody) littermate control and mast cell-deficient *Sash*$^{-/-}$ mice. n = 5–6 mice per group. ****$p < 0.0001$ by unpaired Student's t test.

(G) Number of scratching bouts following i.d. OVA challenge in sensitized (i.v. anti-OVA IgE antibody) WT mice that were pretreated with vehicle or antihistamines olopatadine (OLP, 3 mg/kg; intraperitoneal) and JNJ7777120 (JNJ, 20 mg/kg; subcutaneous injection into the nape) 30 minutes prior to i.d. OVA challenge. n = 4–5 mice per group. *$p < 0.05$ by unpaired Student's t test.

(legend continued on next page)

(H) Schematic of acute itch flares in the passive sensitization model in AD-like disease. Naive mice were topically treated with MC903 on the ear skin from day 0 to day 9 and received i.v. injection of PBS control or anti-OVA IgE antibody on day 8 and day 9. On day 10, i.d. injection of OVA was administered into non-lesional cheek skin of mice. Chronic spontaneous itch and acute itch flares were recorded prior to and following i.d. OVA challenge on day 10, respectively.

(I) Number of scratching bouts prior to i.d. OVA challenge (chronic spontaneous itch; left) and following i.d. OVA challenge (acute itch flares; right) in unsensitized (i.v. PBS) and sensitized (i.v. anti-OVA IgE antibody) WT mice with AD-like disease. n = 4–5 mice per group. N.S., not significant, $^{**}p < 0.01$ by unpaired Student's t test.

(J) Number of scratching bouts prior to i.d. OVA challenge (chronic spontaneous itch; left) and following i.d. OVA challenge (acute itch flares; right) in sensitized (i.v. anti-OVA IgE antibody) littermate control and mast cell-deficient *Sash*$^{-/-}$ mice with AD-like disease. n = 6 mice per group. N.S., not significant by unpaired Student's t test.

Data are represented as mean ± SD.

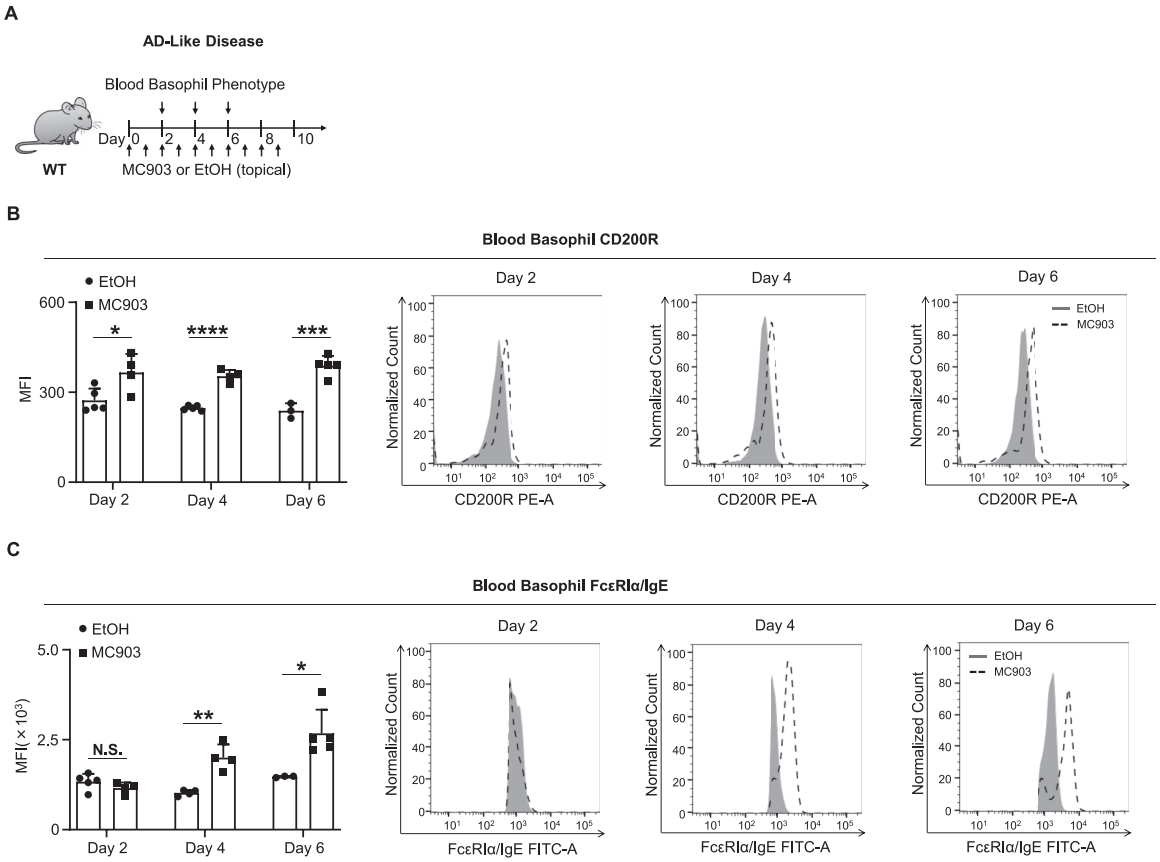

Figure S2. Circulating basophils acquire a distinct phenotype early and sustainably in mice with AD-like disease, related to Figure 2

(A) Schematic of the AD-like disease model. Topical vehicle EtOH control or MC903 was applied to bilateral ear skin of WT mice from day 0 to day 9. Blood basophils from WT mice were assessed for phenotypic alterations on day 2, day 4, and day 6 of the AD-like disease model.

(B and C) CD200R (B) and FcεRIα/IgE (C) expression measured by mean fluorescence intensity (MFI) on blood basophils in EtOH- or MC903-treated WT mice on day 2, day 4, and day 6 of the AD-like disease model. n = 3–5 mice per group. Data are represented as mean ± SD. N.S., not significant, *$p < 0.05$, **$p < 0.01$, ***$p < 0.001$, ****$p < 0.0001$ by unpaired Student's t test.

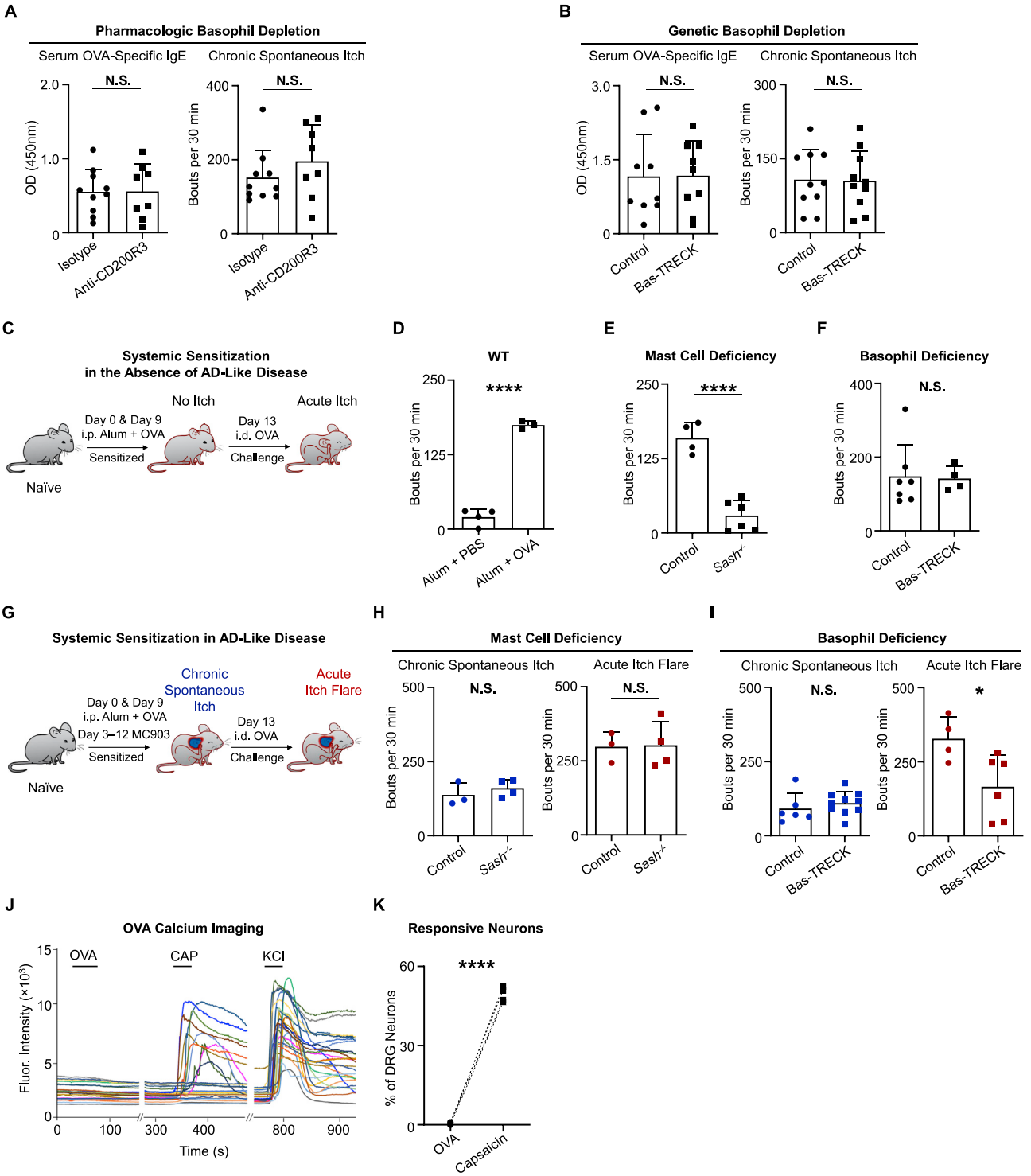

Figure S3. Basophils are dispensable for chronic spontaneous itch but are required for acute itch flares in AD-like disease, related to Figure 4

(A) ELISA quantification of serum OVA-specific IgE (left) and assessment of chronic spontaneous itch (right) in isotype- or anti-CD200R3 monoclonal antibody-administered WT mice on day 10 of the AD-associated acute itch flare model. Scratching behavior was recorded prior to i.d. OVA challenge for chronic spontaneous itch assessment. n = 8–10 mice per group. N.S., not significant by unpaired Student's t test.

(B) ELISA quantification of serum OVA-specific IgE (left) and assessment of chronic spontaneous itch (right) in littermate control and basophil-depleted Bas-TRECK mice on day 10 of the AD-associated acute itch flare model. To quantify chronic spontaneous itch bouts, scratching behavior was recorded prior to i.d. OVA challenge. n = 9–10 mice per group. N.S., not significant by unpaired Student's t test.

(legend continued on next page)

(C) Schematic of Imject Alum (alum) and OVA systemic sensitization model. Naive WT mice received intraperitoneal (i.p.) injection of adjuvant alum and OVA mixture on day 0 and day 9 followed by i.d. OVA challenge into cheek skin and assessment of scratching behavior on day 13.
(D) Number of scratching bouts following i.d. OVA challenge in unsensitized (i.p. alum + PBS) or sensitized (i.p. alum + OVA) WT mice. n = 3–4 mice per group. ****$p < 0.0001$ by unpaired Student's t test.
(E) Number of scratching bouts following i.d. OVA challenge in sensitized (i.p. alum + OVA) littermate control and mast cell-deficient *Sash*$^{-/-}$ mice. n = 4–6 mice per group. ****$p < 0.0001$ by unpaired Student's t test.
(F) Number of scratching bouts following i.d. OVA challenge in sensitized (i.p. alum + OVA) littermate control and basophil-depleted Bas-TRECK mice. n = 4–7 mice per group. N.S., not significant by unpaired Student's t test.
(G) Schematic of acute itch flares in the i.p. alum + OVA systemic sensitization model in the context of AD-like disease. Naive mice received i.p. alum + OVA on day 0 and day 9. From day 3 to day 12, mice were topically treated with MC903 on the ear skin followed by an i.d. injection of OVA into non-lesional cheek skin on day 13. Chronic spontaneous itch and acute itch flares were recorded prior to and following i.d. OVA challenge on day 13, respectively.
(H) Number of scratching bouts prior to i.d. OVA challenge (chronic spontaneous itch; left) and following i.d. OVA challenge (acute itch flares; right) in littermate control and mast cell-deficient *Sash*$^{-/-}$ mice sensitized with i.p. alum + OVA in the context of AD-like disease on day 13. n = 3–4 mice per group. N.S., not significant by unpaired Student's t test.
(I) Number of scratching bouts prior to i.d. OVA challenge (chronic spontaneous itch; left) and following i.d. OVA challenge (acute itch flares; right) in littermate control and basophil-depleted Bas-TRECK mice sensitized with i.p. alum + OVA in the context of AD-like disease on day 13. n = 4–10 mice per group. N.S., not significant, *$p < 0.05$ by unpaired Student's t test.
(J) Representative calcium traces of mouse dorsal root ganglia (DRG) responses to OVA. Calcium responses were measured by fluorescence (Fluor.) intensity (488 nm). Neurons isolated from *Pirt*$^{GCaMP3/+}$ mice were sequentially stimulated with OVA (0.25 mg/mL in calcium imaging buffer), capsaicin (CAP, 500 nM), and KCl (50 mM). Each color trace represents one neuron.
(K) Percentage (%) of OVA-responsive and capsaicin-responsive neurons out of all KCl-responsive neurons. Each data point represents the percent of responsive neurons from one individual *Pirt*$^{GCaMP3/+}$ mouse. n = 4 mice (> 200 neurons each). ****$p < 0.0001$ by paired Student's t test.
Data are represented as mean ± SD.

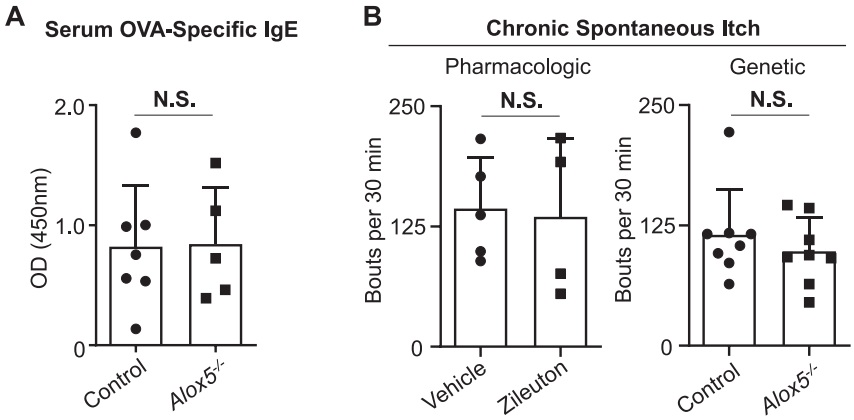

Figure S4. Leukotriene disruption does not affect OVA-specific IgE levels or chronic spontaneous itch, related to Figure 5

(A) ELISA quantification of serum OVA-specific IgE levels in littermate control and *Alox5*$^{-/-}$ mice on day 10 of the AD-associated acute itch flare model. n = 5–7 mice per group.

(B) Assessment of chronic spontaneous itch prior to i.d. OVA challenge on day 10 of the AD-associated acute itch flare model in WT mice that were pre-administered vehicle or zileuton (50 mg/kg; gavage) 60 minutes prior to chronic spontaneous itch assessment (left). Assessment of chronic spontaneous itch prior to i.d. OVA challenge on day 10 of the AD-associated acute itch flare model in littermate control and *Alox5*$^{-/-}$ mice (right). n = 4–8 mice per group.

Data are represented as mean ± SD. N.S., not significant by unpaired Student's t test.

CellPress

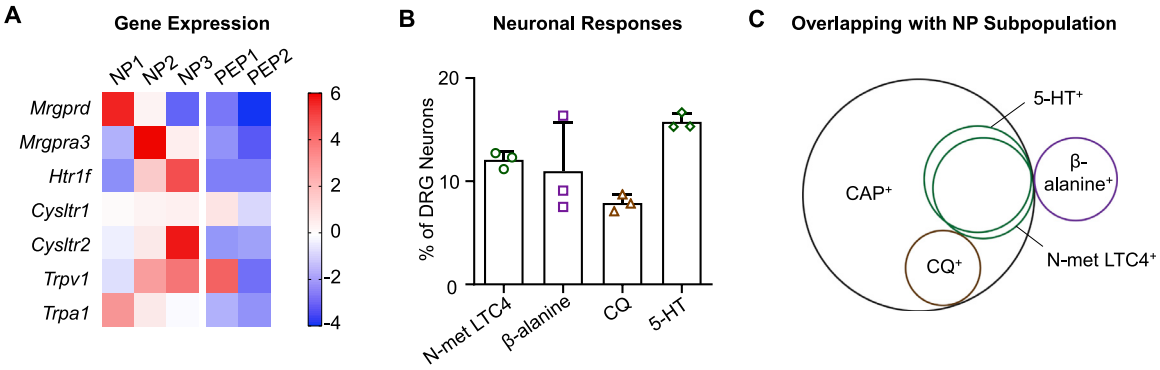

Figure S5. N-met LTC4 activates a subpopulation of itch-specific NP3 neurons, related to Figure 7

(A) Expression of selected genes in mouse DRG neuron populations NP1, NP2, NP3, PEP1 and PEP2 based on single cell RNA-sequencing data. Pruriceptor populations are considered to be NP1, NP2, and NP3, while nociceptors are considered to primarily be in PEP1 and PEP2 population. Full database is available in Usoskin et al. (2015).

(B) Percentage (%) of mouse DRG neurons isolated from *Pirt*$^{GCaMP3/+}$ calcium reporter mice that are responsive to *N*-methyl leukotriene C4 (N-met LTC4, 100 nM), β-alanine (1 mM), chloroquine (CQ, 2 mM), and serotonin (5-HT, 200 μM) out of all KCl-responsive neurons. Each data point represents the percent of neurons that were responsive to a stimulant in an individual mouse. n = 3 mice (> 200 neurons each). Data are represented as mean ± SD.

(C) Representative Venn diagram depicting the overlapping responses of mouse DRG neurons to stimulation with N-met LTC4 (100 nM), β-alanine (1 mM), CQ (2 mM), 5-HT (200 μM), and capsaicin (CAP, 500nM). n > 200 neurons for each test from a *Pirt*$^{GCaMP3/+}$ mouse.

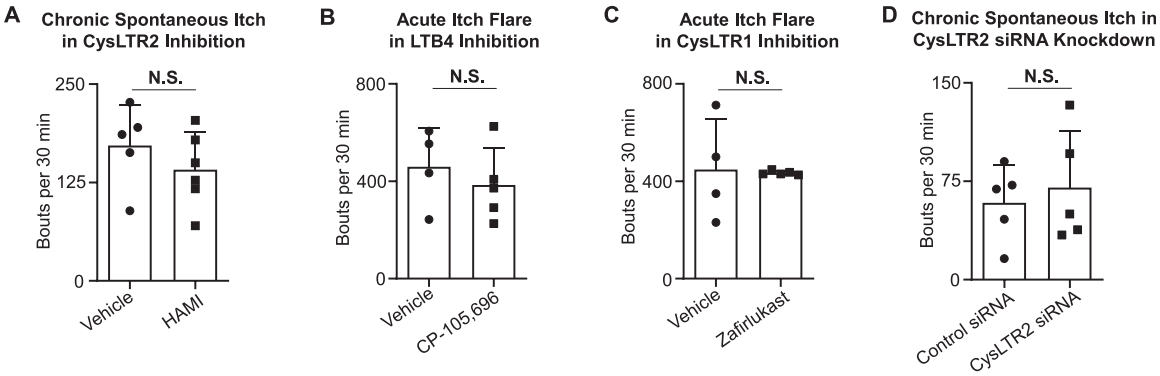

Figure S6. Chronic spontaneous itch is not affected by CysLTR2 inhibition and pharmacologic inhibition of CysLTR1 or LTB4 does not reduce acute itch flares in AD-like disease, related to Figure 7

(A) Assessment of chronic spontaneous itch prior to i.d. OVA challenge on day 10 of the AD-associated acute itch flare model in WT mice that were pre-administered vehicle or the CysLTR2 antagonist HAMI3379 (HAMI, 0.4 mg/kg; i.p.) on day 9 (two doses) and day 10 (1 dose, 60 minutes prior to chronic spontaneous itch assessment). n = 5–6 mice per group.

(B) Number of scratching bouts following i.d. OVA challenge on day 10 of the AD-associated acute itch flare model in WT mice that were pre-administered vehicle or the LTB4 receptor inhibitor CP-105,696 (3 mg/kg; gavage) 60 minutes prior to i.d. OVA challenge. n = 4–5 mice per group.

(C) Number of scratching bouts following i.d. OVA challenge on day 10 of the AD-associated acute itch flare model in WT mice that were pre-administered vehicle or the CysLTR1 antagonist zafirlukast (10 mg/kg; gavage) on day 9 (two doses) and day 10 (1 dose, 60 minutes prior to i.d. OVA challenge). n = 4–5 mice per group.

(D) Assessment of chronic spontaneous itch prior to i.d. OVA challenge on day 10 of the AD-associated acute itch flare model in WT mice that were pretreated with i.c. injections of control siRNA or CysLTR2 siRNA. n = 5 mice per group.

Data are represented as mean ± SD. N.S., not significant by unpaired Student's t test.

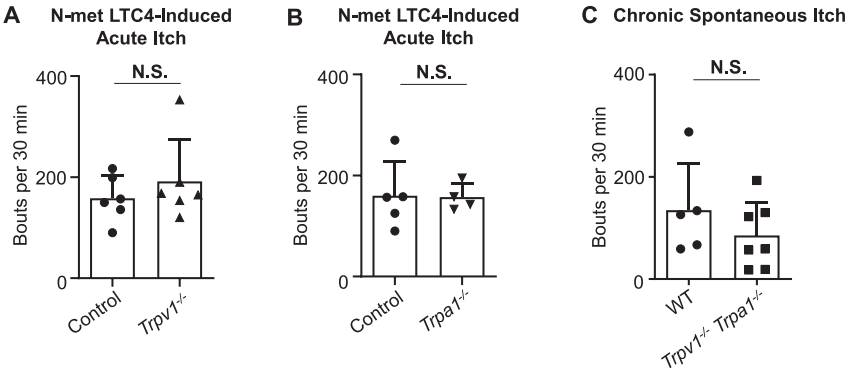

Figure S7. Deletion of TRPV1 or TRPA1 does not reduce N-met LTC4-induced acute itch and compound deletion of TRPV1 and TRPA1 does not affect chronic spontaneous itch associated with AD, related to Figure 7

(A) Number of scratching bouts following i.d. injection of N-met LTC4 (0.75 μg) in naive littermate control and *Trpv1*$^{-/-}$ mice. n = 6 mice per group.

(B) Number of scratching bouts following i.d. injection of N-met LTC4 (0.75 μg) in naive littermate control mice and *Trpa1*$^{-/-}$ mice. n = 4–5 mice per group.

(C) Assessment of chronic spontaneous itch prior to i.d. OVA challenge on day 10 of the AD-associated acute itch flare model in WT and compound *Trpv1*$^{-/-}$ *Trpa1*$^{-/-}$ mice. n = 5–7 mice per group.

Data are represented as mean ± SD. N.S., not significant by unpaired Student's t test.

Cell, Volume *184*

Supplemental Information

A basophil-neuronal axis promotes itch

Fang Wang, Anna M. Trier, Fengxian Li, Seonyoung Kim, Zhen Chen, Jiani N. Chai, Madison R. Mack, Stephanie A. Morrison, Jennifer D. Hamilton, Jinok Baek, Ting-Lin B. Yang, Aaron M. Ver Heul, Amy Z. Xu, Zili Xie, Xintong Dong, Masato Kubo, Hongzhen Hu, Chyi-Song Hsieh, Xinzhong Dong, Qin Liu, David J. Margolis, Marius Ardeleanu, Mark J. Miller, and Brian S. Kim

SUPPLEMENTAL TABLE

Table S1. Characteristics of Healthy Controls and Patients with Atopic Dermatitis, Related to Figure 2

Identity	HC	AD	p value
Number of Participants	12	12	N/A
Age (years)	49.1 ± 16.6	40.4 ± 14.6	0.1878, by unpaired Student's t-test
Sex	10 F, 2 M	9 F, 3 M	> 0.999, by Fisher's exact test
AD Severity (N, %)*			
Clear/Almost Clear	N/A	1 (8.3%)	N/A
Mild	N/A	0 (0)	N/A
Moderate	N/A	7 (58.3%)	N/A
Severe	N/A	3 (25.0%)	N/A
Very Severe	N/A	1 (8.3%)	N/A
Allergy History (N, %)	4 (25.0%)	10 (83.3%)	0.0361, by Fisher's exact test

Abbreviations: AD, atopic dermatitis; F, female; HC, health control; M, male; N/A, not applicable.

*AD severity was evaluated by Patient Oriented Eczema Measure (POEM).